A Rapid *in vivo* Pipeline to Identify Small Molecule Inhibitors of Amyloid Aggregation

Muntasir Kamal[1,2,3*], Jessica Knox[1,2*], Robert I. Horne[4], Om Shanker Tiwari[5], Andrew R. Burns[1,2], Duhyun Han[1,2,6], Dana Laor Bar-Yosef[5], Ehud Gazit[5,7,8], Michele Vendruscolo[4], and Peter J. Roy[1,2,6,9]

1. Department of Molecular Genetics, University of Toronto, Toronto, ON, M5S 1A8, Canada
2. The Donnelly Centre for Cellular and Biomolecular Research, University of Toronto, Toronto, ON, M5S 3E1, Canada
3. Krembil Research Institute, Toronto Western Hospital, University Health Network, Toronto, ON, M5T 0S8, Canada
4. Centre for Misfolding Diseases, Yusuf Hamied Department of Chemistry, University of Cambridge, Cambridge, CB2 1EW, United Kingdom
5. The Shmunis School of Biomedicine and Cancer Research, George S. Wise Faculty of Life Sciences, Tel Aviv University, Tel Aviv 6997801, Israel.
6. Department of Pharmacology and Toxicology, University of Toronto, Toronto, ON, M5S 1A8, Canada
7. Department of Materials Science and Engineering, The Iby and Aladar Fleischman Faculty of Engineering, Tel Aviv University, Tel Aviv 6997801, Israel.
8. Sagol School of Neuroscience, Tel Aviv University, Ramat Aviv, Tel Aviv 6997801, Israel.

*These authors contributed equally to this work

[9]Corresponding Author: Peter J. Roy
Tel: (416) 946-8395
Fax: (416) 978-6885

30 E-mail: peter.roy@utoronto.ca

31

32 **Keywords:** *C. elegans*, pharynx, cuticle, pharyngeal cuticle, chitin, chitosan, Congo red,
33 Thioflavin S, ThS, Eeosin Y, EY, Calcofluor white, CFW, EY, intrinsically disordered
34 proteins, IDPs, amyloid, amyloid disruptors, Aβ42, drug screens, chemical biology

Abstract

Amyloids are associated with over 50 human diseases and have inspired significant effort to identify small molecule remedies. Here, we present a novel *in vivo* platform that efficiently yields small molecule disruptors of amyloid formation. We previously identified small molecules that kill the nematode *C. elegans* by forming membrane-piercing crystals in the pharynx cuticle, which is rich in amyloid-like material. We show here that many of these molecules are known amyloid-binders whose crystal-formation in the pharynx can be blocked by amyloid-binding dyes. Furthermore, we found that amyloid fibrils can seed small molecule crystal formation *in vitro*. These observations suggest that small molecule crystals are seeded by the cuticle's amyloid-like material. We asked whether this phenomenon could be exploited to identify additional molecules that interfere with the ability of amyloids to seed higher-order structures. We screened 2560 compounds and identified 85 crystal suppressors, which we found to be 10-fold enriched in known amyloid disruptors relative to a random set. Of the uncharacterized suppressors, we found 25% to inhibit Ab42 fibril nucleation and/or extension *in vitro*, which is a hit rate that far exceeds other screening methodologies. Hence, screens for suppressors of crystal formation can efficiently reveal small molecules with amyloid-disrupting potential.

53 **Introduction**

54 Previous small molecule screens with the free-living nematode *C. elegans*
55 serendipitously revealed compounds that visibly accumulate within the heads of worms
56 [1-4]. This accumulation can be observed using a low magnification dissection light
57 microscope [5]. We demonstrated that the accumulated small molecules form either
58 birefringent irregular objects, globular non-birefringent spheres, or a mixture of the two,
59 depending on the structure of the compound [5]. Birefringence is an optical property that
60 reveals the subject to harbour repeating units that uniformly alter the angle of incidence
61 of polarized transmitted light. We showed that these birefringent objects: i) are
62 observable within minutes of exposure of the worms to the small molecule; ii) contain
63 the exogenous small molecule; iii) grow over time; iv) are formed exclusively in
64 association with the pharynx cuticle; and v) are not due to the consumption of
65 precipitate in the media by the worm [5,6]. Given their birefringent nature and growth
66 over time, we refer to the birefringent objects as crystals for simplicity's sake, although
67 their exact biophysical nature remains to be determined (Figure 1A-C). The crystals kill
68 younger animals likely because they perforate the plasma membrane of surrounding
69 cells and rapidly grow to occlude the pharynx lumen [5].

70 More recently, we described how the crystals form in tight association with the non-
71 luminal face of the *C. elegans* pharyngeal cuticle [6]. This cuticle is a flexible non-
72 collagenous chitin-rich matrix that is repeatedly shed and rebuilt at each larval stage [7,8].
73 We also constructed a spatiotemporal map for the development of the pharyngeal
74 cuticle of *C. elegans* [9]. That study revealed the pharynx cuticle to be highly enriched with

75 intrinsically disordered proteins (IDPs) and proteins with intrinsically disordered regions
76 (IDRs) [9]. Many of these IDP and IDR-rich proteins have amyloidogenic features that
77 include an enrichment in π-bonding and hydrogen-bonding capabilities, and have
78 protofilament formation propensity [9]. Furthermore, we and others showed that
79 amyloid-binding dyes specifically stain the pharyngeal cuticle [9,10]. Despite these findings,
80 neither transmission electron microscopy (TEM) nor diagnostic tests provide evidence
81 for extended amyloid fibrils within the pharyngeal cuticle [9,11-13], which is consistent with
82 the flexible nature of the cuticle [14,15]. Taken together, these observations indicated that
83 the cuticle is rich in amyloid-like material that lacks the highly ordered nature of amyloid
84 fibrils.

85 Here, we show that molecules that form crystals *in vivo* can indeed form a crystalline
86 lattice *in vitro* through π-bond interactions. We go on to show that over 50% of the 29
87 distinct structural scaffolds that form crystals *in vivo* are reported amyloid binders.
88 Consistent with these observations, we find that, i) nascent crystals distort the amyloid-
89 like material within the cuticle without a concomitant effect on the chitin matrix; ii)
90 Aβ42 fibrils can seed the formation of objects *in vitro* from a small molecule that forms
91 crystals *in vivo*; and iii) worms incubated with the amyloid-binders Congo Red and
92 Thioflavin S can block crystal formation. Collectively, these results suggest that the
93 amyloid-like material in the pharynx cuticle can seed the formation of small molecule
94 crystals.

95 Given that well-characterized amyloid binders can block the seeding of crystals in the
96 pharynx, we wondered whether the crystallization phenomenon could be exploited to

97 identify other small molecules that block the ability of amyloids to seed higher order
98 structures such as amyloid fibrils. We therefore screened 2560 drugs and natural
99 products for those that could suppress crystal formation in the *C. elegans* pharynx. The
100 screen yielded 85 reproducible suppressors, several of which are fluorescent and
101 specifically localize to the cuticle, which is consistent with their expected site of action.
102 The 85 crystal suppressors can be grouped into 45 distinct small molecule scaffolds.
103 Of these 45, one third are previously characterized disruptors of amyloid fibril
104 formation. We tested 44 of the suppressors that have not been previously implicated in
105 amyloid disruption and found that 11 (25%) inhibit Aβ42 aggregation. In total, 40 of the
106 85 suppressors (47%) were shown to disrupt amyloid formation of one type or another,
107 which is a hit rate higher than most previously reported screening methodologies [16-18].
108 We conclude that screens for suppressors of crystal formation within the *C. elegans*
109 pharynx cuticle can enrich for small molecules with amyloid-disrupting potential.

110 **Results**

111 **Crystallizing Molecules are Aromatic, Compact, and Crystalize via π Bond Interactions**

112 We previously identified 38 compounds that form crystals in association with the *C.*
113 *elegans* pharynx cuticle by surveying 238 compounds from our custom library of worm-
114 active (wactive or wact) small molecules [2,5]. We have since identified additional
115 crystalizing molecules from a targeted survey of the wactive library molecules to yield a
116 total of 48 crystallizing compounds (Supplemental Figure 1).

117 To better understand how these 48 crystallizing molecules differ from the 149 true
118 negatives that fail to crystalize, we extended our previous physicochemical analysis to
119 analyze a total of 72 features (Supplemental Table 1). We found no major differences in
120 molecular weight (p=0.75) or hydrophobicity (i.e., cLogP) (p=0.05), and as previously
121 reported [5], the crystallizing molecules have fewer rotatable bonds (p=4.3E-05) and
122 fewer hydrogen-bond donors (p=2.4E-06) than non-crystalizing wactives (Figure 1D).
123 Our more in-depth analysis shows that the crystallizing wactives are highly aromatic
124 (p=2.6E-10) and more compact (i.e., smaller van der Waals volume, p=7.3E-04). A
125 measure that combines these features, called fraction Csp3, reports the ratio of sp3
126 hybridized carbon atoms over the total carbon atom count of the small molecule [19] and
127 reveals the compactness of the crystallizing molecules (p=5.5E-09).

128 To test whether these features are specific to crystallizing molecules from the wactive
129 library, we screened two other libraries for crystallizing molecules. The first library was a
130 custom collection of 1178 small molecules called RLL1200 (Supplementary Datafile 1).
131 The second was the Spectrum library of 2560 drugs and natural products (Microsource

132 Inc). To identify crystalizing molecules from these libraries, we first screened them for
133 those that kill L1 larvae in our standard 6-day viability assay [2], reasoning that crystalizing
134 molecules invariably kill larvae [5] and would be among the hits. We identified 70 lethal
135 molecules from the RLL1200 library and 78 from the Spectrum library. To find
136 crystallizing molecules among these hits, we exploited our previous finding that the *sms-*
137 *5(0)* null mutant resists crystal-induced death by blocking crystal formation [5]. Re-
138 screening the lethal hits against the *sms-5(0)* mutant revealed 16 molecules from
139 RLL1200 and 1 molecule from Spectrum that: i) kill wild type; ii) fail to kill *sms-5(0)*
140 mutants; and iii) form crystals in association with the pharynx (Supplementary Datafile
141 1). The physicochemical features of the RLL1200 crystallizing molecules are not
142 significantly different from those of the wactive crystallizing molecules (p>0.001) (Figure
143 1D; Supplemental Table 1; Supplementary Datafile 1). Statistical analysis was not
144 conducted with the one Spectrum hit, but its properties are similar to the means of the
145 other crystalizing molecules. Hence, compact aromatic properties are common to most
146 crystallizing molecules.
147 Given that aromatic structures are rich in π bonds, we asked whether π bond
148 interactions might play a role in the crystallization of the small molecules *in vitro*. To
149 investigate, we used crystal powder-X-ray diffraction (PXRD) with two exemplar
150 molecules wact-190 and wact-416. Wact-190 crystallized in the triclinic crystal system
151 with the space group P-1, whereas wact-416 crystallized in the orthorhombic crystal
152 system with the space group $Pna2_1$ (Figure 2A-C, 2F-H; Supplemental Table 2;
153 Supplemental Figure 2). The centroids of the aromatic rings for the respective

154 crystalized molecules had distances of 5.0 Å or less, indicating that π-π interactions play
155 a key role in their assembly into higher ordered structures [20] (Figure 2D and I). We
156 compared the crystallization results with their simulated data to validate the bulk phase
157 purity of the crystals. In comparison to the computer-simulated data, the small molecule
158 crystals displayed a similar crystalline nature, peak-pattern matching and single-phase
159 identification, confirming the individual structural purity of the samples (Figure 2E and J;
160 Supplemental Figure 2).
161
162 **Molecules that Induce Crystal Formation in *C. elegans* are Enriched with Amyloid-**
163 **Binding Substructures**
164 To investigate the structural diversity among crystal-forming compounds, we created a
165 structural-similarity network by first reducing each molecule to its core scaffold. We
166 then linked the scaffolds that had a Tanimoto similarity coefficient of 0.8 or more (see
167 methods). This produced a network of 6 clusters that are unconnected with one another
168 and 15 singletons (Figure 3A). Visual inspection of the molecules within the network
169 reveals 30 structurally distinct families (Figure 3A; Supplemental Figure 1).
170 A search of the patent and academic literature using the SciFinder search tool [21]
171 revealed that 15 of the 30 scaffolds (50%) are found in molecules that bind amyloids
172 (pink-outlined nodes in Figure 3A, Supplemental Figure 1, and Supplemental Table 3).
173 For example, scaffolds (a), (k) and close analogs of wact-102 have been shown to bind
174 Aβ42 amyloid aggregates with low nanomolar affinity [22-24]. Scaffold (i) and close analogs
175 of wact-128 and wact-415 were shown to bind prion amyloid aggregates with low

176 nanomolar affinity [25]. In another example, wact-498 is a flavonoid, which is an
177 intensively studied class of molecules that have therapeutic potential for treating
178 amyloid-related neurodegeneration (reviewed [26]). In particular, isoflavone analogs of
179 wact-498 can disrupt Aβ42 plaque formation in a *C. elegans* model of the human disease
180 [27] and were shown to directly bind Aβ42 *in vitro* [28]. The same analysis was performed on
181 62 randomly chosen scaffolds from molecules that do not form crystals [5]. We found only
182 6 scaffolds (10%) that were previously described to bind amyloids (Supplemental Table
183 4). These data suggest that the collection of crystal-forming molecules is enriched with
184 amyloid-associating substructures.
185
186 **Crystals Disrupt the Amyloid-Like Material of the Pharyngeal Cuticle**
187 We sought to better understand how crystal growth perturbs the materials of the
188 cuticle. To investigate, we used cuticle-binding dyes and fluorescent reporters. We
189 previously found that the red-fluorescent Congo red (CR) and blue fluorescent Thioflavin
190 S (ThS), both of which are well-established amyloid-binding dyes [29-32], specifically bind
191 the pharyngeal cuticle [9]. Similarly, the blue-fluorescent Calcofluor white (CFW) and the
192 yellow-red-fluorescent Eosin Y (EY), which bind chitin [33] and its deacetylated derivative
193 chitosan [34] respectively, specifically bind the pharyngeal cuticle [9].
194 We incubated worms in wact-190 and wact-390 (a second crystalizing molecule) for 3
195 hours followed by 2 hours of incubation of the dyes. We found that the amyloid dye
196 patterns are often disrupted by the nascent objects (Figure 4). We also observe a similar
197 pattern in the background where a single IDR-rich protein (ABU-14) is tagged with GFP [10]

198 (Supplemental Figure 3). By contrast, the chitin and chitosan dyes are relatively
199 unperturbed (Figure 4; Supplemental Figure 3). In some instances, the birefringent
200 crystals overlap with amyloid stain (blue arrows, Figure 4). In other cases, there is little
201 overlap between the birefringent signal and the amyloid stain (orange arrows, Figure 4).
202 To control for the possibility that the dyes bind the crystals, we asked whether the
203 dyes bind to *in vitro* precipitated small molecules. None of the dyes fluoresced brightly
204 in association with the *in vitro* precipitated small molecules (Figure 4G). We also
205 examined the dye-staining patterns in the presence of much larger 24-hour old *in vivo*
206 crystals. We found many obvious examples where the larger birefringent signals do not
207 overlap with the CR signal (orange arrows, Supplemental Figure 4). These results suggest
208 that nascent crystals can displace the CR-stained material, which often appears to
209 surround the small crystals. This is consistent with the matrix-like material that
210 surrounds the objects in the TEM images (see Figure 2h for example in [6]. As the crystals
211 grow, their larger mass becomes more distinct from the cuticle and their intimate
212 association with the amyloid-staining material is often lost.
213
214 **Amyloids Likely Seed the Formation of Small Molecule Crystals**
215 As shown above, crystal-forming small molecules are rich in amyloid-binding
216 substructures and that crystals can perturb the amyloid-like material in the pharynx
217 cuticle as they grow. These observations raised the possibility that the amyloid-like
218 material in the pharynx cuticle [9] might seed the formation of the small molecule crystals.
219 If true, then coating the amyloid-like material with well-characterized amyloid-binding

220 dyes might block crystal formation. We tested this idea by first asking whether wact-
221 190-associated lethality of *C. elegans* is suppressed by co-incubating the worms with the
222 amyloid-binding dyes CR and ThS in our standard 6-day viability assay [5]. Indeed, we
223 found that CR and ThS robustly suppress wact-190 lethality whereas the chitin/chitosan-
224 binding dyes do not (Figure 5A). Second, we asked whether the canonical amyloid-
225 binding dyes can suppress wact-190 crystal formation. We incubated CR and ThS, along
226 with CFW and EY with the animals either for 3 hours before incubating the worms with
227 wact-190 for another 3 hours (i.e. a pre-incubation) or at the same time as a 3-hour
228 incubation with wact-190 (i.e. a co-incubation). We found that both CR and ThS
229 suppress crystal formation in both incubation schemes, but that the CFW and EY dyes do
230 not (Figure 5B and 5C). These data suggest that the crystals formed from the exogenous
231 compounds may be seeded by the amyloid-like material in the pharynx cuticle, which
232 can be blocked by other amyloid-interacting compounds.
233 We further investigated the idea that amyloids might seed the small molecule crystals
234 by asking whether Aβ42 fibrils could seed the formation of wact-190 objects *in vitro*.
235 We prepared solutions of Aβ42 at 25 μM and wact-190 at 25, 0.5 and 0.1 μM in PBS and
236 incubated them overnight either alone or in combination with each other at different
237 ratios. The next day, we examined the self-assembled structures by TEM (see Methods).
238 We found objects associated with the Aβ42 fibrils were present in solutions with wact-
239 190 present in either 10-fold more (Figure 6D), 2-fold more (Figure 6C), or 50-fold less
240 than the concentration of Aβ42 (Figures 6G-H), but not 250-fold less (Figures 6K-L) or
241 without wact-190 present (Figures 6A, E, and I). We infer that the objects are self-

242 assemblies of wact-190. Together with the *in vivo* data presented above, these data
243 suggest that amyloids are capable of seeding wact-190 self-assembly into higher order
244 structures.
245
246 **Amyloid Disruptors are Revealed in a Screen for Small Molecule Suppressors of Crystal**
247 **Formation**
248 Above, we show that amyloid-binding probes can block crystal formation. This raised the
249 possibility that screens for small molecules that disrupt crystal formation might yield
250 new amyloid-interacting and/or disrupting molecules. To investigate, we screened
251 Microsource's Spectrum library of 2560 drugs and natural products for those that might
252 suppress crystal formation.
253 We screened the Spectrum library in our standard six-day liquid viability assay
254 whereby multi-well plates are seeded with first larval stage animals (see methods and [2]).
255 We previously established that wact-190's lethality in young larvae is dependent on
256 crystal formation [5]. Control (solvent-only) wells are overgrown with worms after six days
257 (Supplemental Table 5). By contrast, wells with wact-190 (3.75 μM) contain either
258 arrested or dead L1s at the assay endpoint (Supplemental Table 5 and [5]).
259 Screening the Spectrum library molecules at 60 μM yielded 85 hits that: i) suppress
260 wact-190-induced lethality; ii) suppress wact-190 crystal formation ($p<0.05$); and iii) fail
261 to suppress lethality induced by a counter-screen control that does not form crystals
262 (the succinate dehydrogenase inhibitor wact-11 [2]) (Supplemental Table 5). To assess the
263 structural diversity of the suppressors, we built a structural similarity network of the

264 molecules (Figure 7A). A Tanimoto coefficient cut-off of 0.8 and manual inspection
265 revealed 45 distinct core scaffolds, 17 of which are represented by multiple molecules
266 (Figure 7A-B).

267 Informatic analyses of the 85 suppressors revealed that 15 of the 45 scaffold groups
268 (33%) contained at least one molecule known to play a direct role in disrupting amyloid
269 fibril formation (bold outline in Figure 7A; Supplemental Table 5). Most of these
270 scaffolds are enriched among the suppressors relative to the entire Spectrum library
271 (see Figure 7B for *p* values). Of note, a benzaldehyde substructure is significantly
272 enriched among the suppressors (2.8-fold enrichment, *p*=2.3E-14; blue highlight in
273 Figure 7B). Importantly, we found that several of the suppressors are fluorescent and of
274 these, all specifically stain the pharyngeal cuticle (Figure 7C and Supplemental Figure 5).

275 We investigated whether the set of 85 wact-190 suppressors is enriched for amyloid
276 disruptors relative to the molecules within the Spectrum library. The lack of a
277 comprehensive database of previously characterized small molecule amyloid disruptors
278 precluded a systematic analysis. We therefore randomly selected 100 molecules from
279 the remaining Spectrum molecules to further investigate. We used the same analytical
280 approach that we employed for the 85 Spectrum suppressors. We first assembled the
281 random molecules into a structural similarity network, revealing 75 structurally-distinct
282 scaffolds (11 clusters plus 64 singletons) (Supplemental Figure 6A). We then investigated
283 the literature for evidence of the ability to disrupt amyloid fibril formation for each of
284 the 100 random molecules (see methods). Two of the 75 core scaffolds (3%) had one
285 molecule shown to be a disruptor of amyloid fibril formation (Supplemental Figure 6B).

286 From this limited analysis, we found that the 85 Spectrum suppressors are over 10-fold
287 enriched in amyloid disruptors relative to the randomly selected set.
288
289 **Small Molecule Suppressors of Crystal Formation Inhibit Aβ42 Fibril Formation**
290 The above results suggest that the mechanism by which molecules suppress crystal
291 formation is intimately related to amyloid disruption. We therefore asked whether any
292 of the molecules for which we could not find literature-based evidence for amyloid
293 disruption have such capability. While different suppressors have been shown to disrupt
294 different types of amyloids (Supplemental Table 5), we focused on Aβ42 for reasons of
295 convenience [35,36]. We measured the incubation time by which Aβ42 fibril formation
296 reaches saturation and asked which molecules are capable of significantly (p<0.05)
297 extending the half-time of saturation by at least 50% in a standard assay [35]. Of the eight
298 molecules previously shown to disrupt amyloids, 3 inhibited Aβ42 fibril formation in our
299 assay (Figure 7A, Supplemental Table 5), indicating that not all published results
300 translate to this specific assay. Of the 44 unknowns tested, 11 (25%) inhibited Aβ42 fibril
301 formation (Figures 7A, D-H, Supplemental Table 5). Follow up analyses on the hits
302 shown in Figure 7E-H shows that Candesartan is a specific nucleation inhibitor while the
303 other molecules inhibit either nucleation and/or elongation. Importantly, all of these
304 inhibitory mechanisms require fibril binding (Supplemental Figure 7). Hence, the ability
305 of a small molecule to suppress crystal formation *in vivo* is predictive of its ability to
306 inhibit amyloid fibril growth *in vitro*.
307

308 **A Scaffold's Ability to Crystalize or Suppress Crystallization is Interchangeable**

309 A comparison of the structures of crystallizers and suppressors revealed that the former
310 have fewer hydrogen-bond donors than the latter and completely lacked hydroxyl
311 groups (p<1E-10) (Figure 8A-B). The crystallizers are also more halogenated than the
312 suppressors (Figure 8C). We also found that some crystallizers share the identical
313 scaffold as some suppressors. For example, the scaffolds of the wact-128 and wact-498
314 crystallizers are identical to that of oxyclozanide and koparin crystal suppressors,
315 respectively (Figure 8D). In addition, the scaffold of the wact-415 crystallizer is similar to
316 that of ThS, which also suppresses crystal formation (Figure 8D). These observations
317 raised the possibility that both classes of molecules (crystallizers and suppressors)
318 compete for the same environment within the cuticle.

319 We tested whether we could convert a crystalizing molecule into a suppressor, and a
320 suppressor into a crystallizer, by altering the abundance of hydroxyl and halogen
321 decorations on the respective core structures. To do this, we searched the ZINC
322 database of the world's commercially available molecules [37] for close structural analogs
323 of the 85 suppressors that lacked hydroxyl groups and are halogenated. We screened 33
324 available analogs of 6 different suppressors. We found that 11 (33%) of these molecules
325 induced object formation within the pharynx in at least 25% of the population
326 (Supplemental Table 6; Figure 8E). This percentage is comparable to the 36% of
327 molecules that induce object formation from our heavily biased collection of worm
328 bioactive small molecules [5]. Second, we tested 25 hydroxylated analogs of 10 different
329 crystalizing small molecules for their ability to suppress the lethality associated with

330 crystal-forming wact-190. Five of the 25 hydroxylated crystallizers (20%) suppress wact-
331 190 lethality, and all of these suppress wact-190 crystal formation ($p<0.05$)
332 (Supplemental Table 7; Figure 8F). We conclude that select core small molecule
333 structures can be pushed towards crystal formation or its suppression by changing the
334 relative abundance of halogens and hydroxyls that decorate the molecule. These data
335 further supports the model that crystallizers and suppressors likely compete for the
336 same niche.

337 Finally, we tested the five converted suppressor molecules in the Aβ42 fibril
338 formation assay and found that the most robust suppressor (OC-17) robustly inhibited
339 Aβ42 fibril formation (Figure 8G; Supplemental Table 7; Supplemental Figure 7E).
340 Hence, converting crystallizers into suppressors is another route with which to identify
341 amyloid disruptors.

342 **Discussion**

343 **Insights into Crystal Formation within the *C. elegans* Pharynx Cuticle**

344 Here, we have described our investigation into why some small molecules crystalize
345 within the cuticle of the *C. elegans* pharynx. We found that: i) many crystal-forming
346 molecules have a core scaffold known to bind amyloid; ii) crystals can displace amyloid-
347 like material within the pharyngeal cuticle; iii) other molecules that are known to bind
348 amyloids can block crystal formation; iv) molecules that block crystal formation
349 specifically localize to the tissue where crystals form; and v) Aβ42 fibrils can seed the
350 formation of wact-190 objects *in vitro*. Together with our previous work that shows the
351 pharynx cuticle to be rich in amyloid-like material [9], these observations suggest that the
352 amyloid-like material within the pharynx cuticle seed the formation of crystals.

353 We can speculate in general terms as to how the amyloid-like material in the pharynx
354 cuticle might seed small molecule crystals. Our physicochemical analyses of crystalizing
355 compounds show that they are rich with π bonding capability, hydrogen bond acceptors,
356 and polar surface areas (this work and [5]). Indeed, our *in vitro* analysis also shows that π
357 bond interactions likely play a key role in the ability of these molecules to crystalize
358 within the pharynx. Concomitant with its amyloid-like nature [38,39], pharynx cuticle
359 proteins are highly enriched in π-bonding capability relative to other tissue proteomes in
360 *C. elegans* and is only surpassed by the collagens [9]. Furthermore, the pharynx secretome
361 is uniquely rich with polar uncharged residues with hydrogen bond donor capability (i.e.,
362 Ns, Qs, Ss, Ts, and Ys) ((p<1E-11) [9]). Hence, the unique complementarity between the

363 proteins within the pharyngeal cuticle and the crystal-forming compounds likely
364 facilitates the seeding of small molecule crystals.
365 Small molecule crystallization is restricted to the pharyngeal cuticle [5], yet the
366 collagens (which are highly abundant within the body cuticle) are also rich in π-bonding
367 capability [9]. Hence, there are likely additional properties of the pharynx cuticle beyond
368 its amyloid-like nature that creates the unique niche that facilitates crystal formation.
369 Indeed, our recent work shows that polar lipids within the pharynx cuticle likely act as a
370 sink to concentrate the hydrophobic molecules that go on to crystallize [6].
371 A model of crystal formation emerges upon considering these and other
372 observations. First, polar lipids within the pharynx cuticle likely act as a sink to
373 concentrate hydrophobic small molecules, including those that go on to crystallize [6].
374 Once concentrated, the amyloid-like material within the pharynx cuticle seeds the
375 crystallization of small molecules that are capable of interacting with the amyloid-like
376 material. Many of the molecules that suppress crystal formation have similar properties
377 to the crystallizing molecules except that they are rich in hydroxyl groups and therefore
378 cannot crystalize themselves. Instead, they mask the niche to prevent the seeding of
379 crystals from small molecules that would otherwise do so.
380
381 **Crystal Formation can be Exploited to Identify Candidate Amyloid Inhibitors**
382 Through this investigation, we discovered that the phenomenon of small molecule
383 crystal formation can be readily exploited to identify candidate inhibitors of amyloid
384 growth. Our screen of just over 2500 small molecules for those that can suppress crystal

385 formation yielded 85 reproducible hits. One third of these were previously known
386 inhibitors of amyloid formation. For example, the heme and chlorophyl precursor
387 protoporphyrin IX, its synthetic derivative haematoporphyrin, and chlorophyllide-Cu are
388 the only porphyrins contained within the Spectrum library, and all three were found to
389 suppress crystal formation. Multiple studies have shown that porphyrins suppress
390 amyloid formation both *in vivo* and *in vitro* and act through direct interaction with
391 amyloidogenic proteins [40-42]. The porphyrin ring is thought to disrupt the intrapeptide π-
392 π interactions of the amyloidogenic peptide that is necessary to achieve superstructure
393 [42]. The porphyrins may suppress crystal formation by disrupting the ability of the
394 amyloid-like material to seed crystals or may disrupt the small molecule crystallization
395 itself.
396 A second common suppressor class are the flavonoids, which are a large class of
397 polyphenolic secondary metabolites synthesized by plants [43]. Many flavonoid structures
398 have been shown to antagonize amyloid formation *in vitro* [44-46], in culture [47], and *in vivo*
399 [48-50]. Poor bioavailability may contribute to a lack of flavonoid-based therapies in the
400 clinic, although converting anti-amyloid flavonoids into prodrugs may circumvent
401 absorption barriers [51]. Flavonoid interaction with Aβ42 is driven by hydrophobic and
402 hydrogen bond interactions that antagonize the ability of Aβ42 to adopt a β-sheet
403 secondary structure [52]. Whether the flavonoids interact with amyloidogenic proteins
404 within the cuticle in a similar way to suppress crystallization remains to be determined.
405 Upon testing 44 small molecules not known to us at the time to disrupt amyloid
406 formation, we found that 25% disrupt Aβ42 aggregation. This hit rate is far higher than

407 that previously reported for Aβ42 (0.4%) [16] or α-synuclein (<0.01%) [18]. Notably, *C.*
408 *elegans* screens for suppressors of crystal-induced death are inexpensive and high-
409 throughput. Furthermore, the *in vivo* environment in which suppressors must act is
410 complex and, relative to other *in vitro* assays, may better approximate the environment
411 in which anti-amyloid compounds must act. Hence, screens for molecules that suppress
412 crystal-induced lethality in *C. elegans* represent a novel and efficient approach to enrich
413 for molecules that might have utility against human amyloid formation.
414

415 **Methods**

416 ***C. elegans* Culture, Strains and Microscopy**

417 *C. elegans* strains were cultured and synchronized as previously described [5]. Six day
418 viability assays were conducted as previously described [2]. The wild type N2 Bristol strain
419 was used (obtained from the *C. elegans* genetic Centre); NQ824 qnEx443[Pabu-14:abu-
420 14:sfGFP; rol-6(d); unc-119(+)], which was a kind gift from David Raizen [10], was
421 integrated into the genome in our lab as *trIs113*. For all imaging, a Leica DMRA
422 compound microscope with a Qimaging Retiga 1300 monochrome camera was used.
423 Before mounting worms on a 3% agarose pad for imaging, worms are washed 3X with
424 M9 buffer and paralyzed with 50 mM levamisole or 30 mM NaN_3. Dye staining
425 experiments were performed as previously described [9].

426

427 **Identification of Crystallizing Small Molecules and Crystal Counts**

428 The RLL1200 library of 1178 commercially available analogs of *C. elegans*-lethal
429 molecules was assembled and purchased from ChemBridge (Supplemental Data File 1).
430 This library was screened at 30 µM in liquid NGM media against synchronized *C. elegans*
431 L1 larvae and *Rhabditophanes diutinus* [53] as previously described [2], with approximately
432 20 L1s plated per well of a 96-well plate. The final volume in each well was 100 µL and
433 the DMSO concentration was 0.3% v/v. After 6 days of incubation at 25°C the number of
434 living worms in each well was quantified. Molecules that killed *C. elegans* N2 and
435 *Rhabditophanes* were tested for resistance in *C. elegans sms-5(ok2498)* mutants at 1.9,
436 7.5, and 30 µM. Crystal counts were performed as previously described [5].

437

438 **Characterization of the Structure of wact-190 and wact-416 *in vitro* Crystals**

439 Both wact-190 and wact-416 crystal powder samples were deposited on a quartz zero-
440 background sample holder. The sample was loaded in a 0.7 mm diameter capillary, to
441 avoid preferment orientation. The powder X-ray diffraction (PXRD) pattern was
442 collected using a Bruker D8 Discover diffractometer (Bruker, Germany) equipped with
443 Goebel's mirrors to create a θ:θ parallel beam geometry with a sealed X-ray tube source
444 with a copper anode (40 Kv, 40 mA) and a LYNXEYE XE linear detector. The diffraction
445 patterns were collected between 5 and 60° 2θ with step 0.02° 2θ for 4 seconds per step
446 [54]. The cell indexing was performed by TOPAS 5.0 software, using the LSI-Index
447 algorithm [55]. The structure resolution was obtained by using the simulated annealing
448 method in EXPO2014 [56]. The founded structure was refined by the Rietveld Method
449 using GSAS-IIin order to precisely refine the atomic positions [57]. The CIF files obtained
450 from the above method and structures were solved using Mercury software.

451

452 **Transmission Electron Microscopy (TEM) of Aβ42 and wact-190 *in vitro* Crystals**

453 5 mM of each of Aβ42 and wact-190 were dissolved in pure DMSO and heated at 55 ^{o}C
454 for 2 minutes for complete dissolution. Thereafter, all molecules were further diluted in
455 1X PBS to prepare a final concentration of 25 µM. This solution mixture was further
456 heated at 90 °C for 3 hours, followed by a vortex and the mixture was then allowed to
457 gradually cool down overnight that resulted in self-assembled structures in some cases.

458 The combinations used for Aβ42 plus wact-190 were 1:1, 1:2, 1:5, and 1:10 ratios.
459 Uncombined Aβ42 and wact-190 were used as controls (25 µM in 1X PBS). The self-
460 assembled samples of all three (5 µL, 25 µM in 1X PBS) were drop cast on a 400-mesh
461 carbon-stabilized Formvar-coated Cu grid (Ted Pella, California, USA). The sample was
462 allowed to bind the surface for 2 minutes and then the excess sample was removed
463 using a lint-free tissue, dried at room temperature, and imaged. Sample morphology
464 was visualized using a JEM-1400 TEM (JEOL, Tokyo, Japan) accelerating at 80 kV [54].
465

466 **Identification of Chemical Suppressors of Crystal-Induced Death and Crystal Formation**

467 To identify chemical suppressors of crystal-induced death, the Spectrum Collection
468 (MicroSource Discovery Systems Inc.) of 2560 approved drugs and natural products was
469 screened at a concentration of 60 µM in the background of 3.75 µM wact-190. This
470 concentration of wact-190 results in crystal formation in the pharynx causing *C. elegans*
471 N2 to arrest at the L1 stage. This screen was performed in liquid NGM media as
472 previously described [2], with approximately 20 N2 L1s plated per well of a 96-well plate.
473 The final volume in each well was 50 µL and the DMSO concentration was 0.8% v/v.
474 After 6 days of incubation at 20°C the number adult and larval worms that have
475 progressed from arrested L1 stage was quantified. Hits that suppressed the wact-190
476 crystal-induced L1 arrest were retested against solvent control, wact-190, and the non-
477 crystal forming lethal molecule wact-11 at 10 µM (see [2]) using the same method
478 described above. Hits were further investigated for their ability to suppress crystal
479 formation by co-incubating 3.75 µM of wact-190 and 60 µM of the suppressor with wild

480 type animals in 96-well plate format. The fraction of animals with birefringent crystals
481 was then counted at 100X magnification 48 hours later, counting 20 animals per sample
482 per trial on average.
483
484 **Chemoinformatic Network Analysis, Network Display, Small Molecule Art, and**
485 **Informatic Analyses**
486 Structural similarity networks were constructed based on pairwise similarity scores
487 calculated as the Tanimoto coefficient of shared FP2 fingerprints. Pairwise similarity
488 scores were calculated using OpenBabel (http://openbabel.org) and the networks were
489 visualized using Cytoscape [58] as previously described [2]. For each network generated, a
490 range of Tanimoto coefficient cut-offs were tested to determine which cut-off yielded a
491 network that clustered obvious structural analogs together as determined by manual
492 inspection. Suppressors were analysed for the presence of substructures (Figure 4b)
493 using Filter-it version 1.0.2 from Silicos-it. Structures were drawn using ChemDraw
494 (PerkinElmer Informatics). A random Spectrum network (Supplemental Figure 5) was
495 generated by assigning all molecules within the Spectrum library a random number
496 using excel, then sorting the molecules in order of the random number, then choosing
497 the top 100 molecules that did not include any of the 85 Spectrum suppressors.
498 We investigated whether the crystalizing molecules and a randomly selected set of
499 true negatives (that fail to robustly form crystals [5]) were previously characterized to
500 interact with amyloids using the SciFinder Scholar tool [21]. To do this, we first assembled
501 the crystalizing molecules into 29 groups based on distinct scaffolds and ensured that

502 our set of 62 true negatives represented 62 distinct core scaffolds (within the set of true
503 negatives). We then reduced each group (or single molecule if it was not part of a group)
504 to its core scaffold structure by removing hydroxyl groups, halogens, or substructures
505 that were not in common to all members of the group. With the resulting core scaffold
506 structures, we first searched SciFinder for any molecule that contained that core
507 scaffold. With these resulting molecules, we then searched the associated biological
508 literature abstracts within SciFinder for the term 'amyloid'. Because of the simplicity of
509 some core scaffolds, the number of respective analogs and associated abstracts
510 numbered in the tens of thousands. In these cases, we instead first chose one molecule
511 from the group (or the single molecule if it was not part of a group) and searched
512 SciFinder for analogs with >80% identity. This reduced the number of relevant structures
513 and associated literature to search and kept the focus on closely related structures.
514 Which of the two tactics was employed is indicated in the relevant Supplementary Table
515 and Supplementary Data File for each scaffold group (or single molecule). Abstracts
516 containing the term 'amyloid' were read (and where unclear, the associated literature
517 was read) to ensure that evidence of either direct amyloid interaction *in vitro* was being
518 measured or that if *in vivo* samples were being analyzed, staining that was coincident
519 with amyloid structures was being measured. Evidence relying solely on the reduction of
520 amyloids *in vivo* were not considered 'hits' because of potential indirect mechanisms.
521 The PubMed IDentification numbers (PMIDs) and/or patent numbers of the 'hits' are
522 reported in the associated Supplementary Tables and Supplementary Data File.

523 We analyzed both the list of 85 Spectrum suppressors of crystal formation and the
524 100 randomly chosen molecules by searching that compound and the word 'amyloid' in
525 both a PubMed search and a Google search. We inspected the search results for
526 evidence that the molecule of interest had a demonstratable inhibitory effect on
527 amyloid formation *in vitro*, with or without supporting *in vivo* evidence. *In vivo* or *in*
528 *silico* evidence of a decrease in fibril abundance without evidence of a direct effect was
529 excluded from consideration. Molecules that lacked evidence for a direct effect, but had
530 close structural analogs that have a demonstratable inhibitory effect on fibral formation
531 were also excluded from further consideration.
532 To identify hydroxylated analogs of the crystallizing molecules and reduced analogs of
533 the suppressors, Open Babel [59] was used for the analog searches. Using SmiLib v2.0 [60], a
534 virtual library of approximately 55,000 variably hydroxylated analogs of 161 distinct
535 crystallizing molecules was generated, as well as a virtual library of approximately
536 950,000 de-hydroxylated and variably halogenated analogs of 12 distinct crystal
537 suppressor molecules. The 55K and 950K virtual libraries were de-duplicated and
538 independently combined with de-duplicated and de-salted versions of MolPort's All
539 Stock Compounds Database and the ZINC In-Stock Database [37]. A duplicate search of
540 these combined datasets revealed 34 crystallizer analogs and 88 crystal suppressor
541 analogs that were available for purchase from MolPort. These analogs were further
542 filtered by price, real availability, redundancy among parent Spectrum suppressors, and
543 aqueous solubility, leaving 26 crystallizer analogs and 33 crystal suppressor analogs to
544 be assayed.

545

546 **Dye Suppression Assays**

547 To test for the ability of dyes to suppress wact-190-induced worm lethality, 80 µL of
548 NGM containing HB101 bacteria (OD_{600} = 1.8-2.2) and 3.75 µM wact-190 was added to
549 each well of a 96-well plate, to which each dye was pinned (pinner model VP381N, V & P
550 Scientific, Inc) to a final concentration of 0, 0.94, 1.88, 3.75, 7.5, 15, 30, 60, 120, 240,
551 480 and 960 µM, in quadruplicates. 20 µL of M9 containing synchronized wildtype L1s
552 were then added to each well at ~50 L1/well. Three sets of controls were simultaneously
553 set up: wact-190 + DMSO (or 70% ethanol) (no dye), DMSO + dye (no wact-190) and
554 DMSO + DMSO (or 70% ethanol) (no wact-190, no dye). All samples were set up in
555 quadruplets (Day 0) and incubated at 20°C in a shaker at 200 rpm. Worm viability was
556 scored on Day 6.

557 To test for the ability of dyes to suppress wact-190-induced crystal formation,
558 synchronized wildtype young adults were added (~ 1,000 worms in 50 µL) to a 1.5 mL
559 Eppendorf tube containing 500 µL NGM buffer and bacteria. Adult worms were either (i)
560 pre-incubated for 3 hours with 60 µM or 1200 µM of each dye or solvent (DMSO) only,
561 rinsed 3X with M9 buffer then incubated with 60 µM wact-190 in a fresh Eppendorf
562 tube, or (ii) co-incubated for 3 hours with 60 µM or 1200 µM of each dye (or solvent)
563 and 60 µM wact-190. Crystal formation was recorded by observing the birefringence of
564 the wact-190 crystals both in the presence and absence of the dye. wact-190 crystal
565 formation was compared with a negative control (no wact-190), that yielded no such
566 birefringence. All observations and imaging were carried out using 40X objective lens of

567 Leica DMRA2 compound microscope. The amount of birefringence was quantified using
568 Fiji/ImageJ software. 10-20 worms per sample were analyzed in 3 biological trials.
569
570 ***In vitro* Crystal Signal Emission Controls with and without Dye Staining**
571 To test for signal emission of wact-190 or wact-390 crystals, as detected with our
572 fluorescent microscopy filter sets, 3 µL of a 10 mM wactive stock was first added to 7 µL
573 of water and mixed in a microcentrifuge tube, then directly added to a microscope glass
574 slide and coverslip applied. The appearance and birefringence of the formed crystals
575 were observed under differential interference contrast (DIC), birefringence, and
576 fluorescence filter sets.
577 To test for whether the dyes specifically bind the *in vitro* precipitated crystals, the
578 same procedure was followed as above, but each dye was added at a final concentration
579 that was used in the dye staining experiments after the wactive precipitated in water.
580 Correlation between crystal birefringence (bright white dots in a dark background) and
581 dye fluorescence in their respective fluorescence channels was examined. All
582 observations were made using the 10X objective lens of the Leica DMRA2 compound
583 microscope.
584
585 **Aβ42 Aggregation Assay**
586 *Recombinant Aβ42 expression* - The recombinant peptide MDAEFRHDSGY EVHHQKLVFF
587 AEDVGSNKGA IIGLMVGGVV IA, here called Aβ42, was expressed in the *E. coli* BL21 Gold
588 (DE3) strain (Stratagene, CA, U.S.A.) and purified as described previously [35]. Briefly, the

589 purification procedure involved sonication of *E. coli* cells, dissolution of inclusion bodies
590 in 8 M urea, and ion exchange in batch mode on diethylaminoethyl cellulose resin
591 followed by lyophilisation. The lyophilised fractions were further purified using Superdex
592 75 HR 26/60 column (GE Healthcare, Buckinghamshire, U.K.) and eluates were analysed
593 using SDS-PAGE for the presence of the desired peptide product. The fractions
594 containing the recombinant peptide were combined, frozen using liquid nitrogen, and
595 lyophilised again.

596 *Aβ42 aggregation kinetics and fibril preparation* - Solutions of monomeric Aβ42 were
597 prepared by dissolving the lyophilized Aβ42 peptide in 6 M guanidinium hydrocholoride
598 (GuHCl). Monomeric forms were purified from potential oligomeric species and salt
599 using a Superdex 75 10/300 GL column (GE Healthcare) at a flowrate of 0.5 mL/min, and
600 were eluted in 20 mM sodium phosphate buffer, pH 8 supplemented with 200 µM EDTA
601 and 0.02% NaN_3. The centre of the peak was collected and the peptide concentration
602 was determined from the absorbance of the integrated peak area using extinction
603 coefficient ε280 = 1490 l Mol^{-1} cm^{-1}. The obtained monomer was diluted with buffer to
604 the desired concentration and supplemented with 20 µM Thioflavin T (ThT) from a 2
605 mM stock. Each sample was then pipetted into multiple wells of a 96- well half-area,
606 low-binding, clear bottom and PEG-coated plate (Corning 3881), 80 µL per well, in the
607 absence and the presence of different molar-equivalents of small molecules (1% DMSO).
608 Assays were initiated by placing the 96-well plate at 37 ºC under quiescent conditions in
609 a plate reader (Fluostar Omega, Fluostar Optima or Fluostar Galaxy, BMGLabtech,

610 Offenburg, Germany). The ThT fluorescence was measured through the bottom of the

611 plate using a 440 nm excitation filter and a 480 nm emission filter.

612

613 **Statistics and Graphs**

614 Except where indicated, statistical differences were measured using a two-tailed

615 Students T-test. Dot plots were generated using Prism 8 graphing software.

616 **Animal Ethics Statement**

617 We (the authors) affirm that we have complied with all relevant ethical regulations for
618 animal testing and research. Given that our experiments focused exclusively on the
619 invertebrate nematode worm *C. elegans*, no ethical approval was required for any of the
620 presented work.

621

622 **Data Availability Statement**

623 Any primary data generated or analyzed during this study that are not included in this
624 published article and its supplementary information files are available upon request.

Acknowledgements

We thank David Hall, Zeynep Altun, and Chris Crocker at WormAtlas for permission to modify Worm Atlas schematics. WormAtlas is funded by NIH OD 01943 to D.H. Hall. This work is supported by CIHR grants (153024 and 173448) and a CRC to PJR, UKRI grants (10059436, 10061100) to MV and RIH, and a John Templeton Foundation Grant to DLB-Y and EG. The opinions expressed in this publication are those of the authors and do not necessarily reflect the views of the John Templeton Foundation.

Author Contributions

PJR and MK found that crystals form in the pharyngeal cuticle. MK performed the microscopy and associated quantification. JK performed additional small molecule screens that revealed new crystal-forming compounds, performed the screen of the Spectrum library for suppressors of crystal-induced death and follow-up work, and performed the network analyses. ARB designed the novel 1,178-compound custom library and identified the crystallizer and suppressor analogs. RIH under the guidance and funding of MV, performed the Ab42 fibril inhibition assay. OST, under the guidance and funding of DLB-Y and EG, determined the structure of wact-190 and wact-416 *in vitro* crystals and showed that Aβ42 fibrils can nucleate wact-190 objects. DH determined whether the fluorescent Spectrum suppressors specifically stain the pharyngeal cuticle. PJR supervised, coordinated and secured funding for the project, composed the display items and wrote the manuscript with the help of co-authors.

647 **Competing Interests**

648 RIH is a consultant of WaveBreak Therapeutics (formerly Wren Therapeutics). MV is a

649 founder of WaveBreak Therapeutics.

650 **Literature Cited**

651 1 Kwok, T. C. *et al.* A small-molecule screen in C. elegans yields a new calcium
652 channel antagonist. *Nature* **441**, 91-95 (2006).
653 2 Burns, A. R. *et al.* Caenorhabditis elegans is a useful model for anthelmintic
654 discovery. *Nat Commun* **6**, 7485, doi:ncomms8485 [pii]
655 10.1038/ncomms8485 (2015).
656 3 Risi, G. *et al.* Caenorhabditis elegans Infrared-Based Motility Assay Identified
657 New Hits for Nematicide Drug Development. *Vet Sci* **6**,
658 doi:10.3390/vetsci6010029 (2019).
659 4 Galford, K. F. & Jose, A. M. The FDA-approved drugs ticlopidine, sertaconazole,
660 and dexlansoprazole can cause morphological changes in C. elegans.
661 *Chemosphere* **261**, 127756, doi:10.1016/j.chemosphere.2020.127756 (2020).
662 5 Kamal, M. *et al.* The marginal cells of the Caenorhabditis elegans pharynx
663 scavenge cholesterol and other hydrophobic small molecules. *Nat Commun* **10**,
664 3938, doi:10.1038/s41467-019-11908-0 (2019).
665 6 Kamal, M. *et al.* PGP-14 Establishes a Polar Lipid Permeability Barrier within the
666 C. elegans Pharyngeal Cuticle. *PLoS Genet* **19(11):e1011008**,
667 doi:10.1371/journal.pgen.1011008 (2023).
668 7 Cox, G. N., Kusch, M. & Edgar, R. S. Cuticle of Caenorhabditis elegans: its isolation
669 and partial characterization. *J Cell Biol* **90**, 7-17 (1981).
670 8 Altun, Z. F. & Hall, D. H. in *WormAtlas* (2020).
671 9 Kamal, M. *et al.* A spatiotemporal reconstruction of the C. elegans pharyngeal
672 cuticle reveals a structure rich in phase-separating proteins. *Elife* **11**,
673 doi:10.7554/eLife.79396 (2022).
674 10 George-Raizen, J. B., Shockley, K. R., Trojanowski, N. F., Lamb, A. L. & Raizen, D.
675 M. Dynamically-expressed prion-like proteins form a cuticle in the pharynx of
676 Caenorhabditis elegans. *Biol Open* **3**, 1139-1149, doi:10.1242/bio.20147500
677 (2014).
678 11 Wright, K. A. & Thomson, J. N. The buccal capsule of Caenorhabditis elegans
679 (Nematodea:Rhabditoidea): an ultrastructural study. *Canadian Journal of*
680 *Zoology* **59**, 1952-1961 (1981).
681 12 White, J. G., Southgate, E., Thomson, J. N. & Brenner, S. The structure of the
682 nervous system of the nematode Caenorhabditis elegans. *Philos Trans R Soc Lond*
683 *B Biol Sci* **314**, 1-340, doi:10.1098/rstb.1986.0056 (1986).
684 13 Sparacio, A. P., Trojanowski, N. F., Snetselaar, K., Nelson, M. D. & Raizen, D. M.
685 Teething during sleep: Ultrastructural analysis of pharyngeal muscle and
686 cuticular grinder during the molt in Caenorhabditis elegans. *PLoS One* **15**,
687 e0233059, doi:10.1371/journal.pone.0233059 (2020).
688 14 Huang, K. M., Cosman, P. & Schafer, W. R. Automated detection and analysis of
689 foraging behavior in Caenorhabditis elegans. *J Neurosci Methods* **171**, 153-164,
690 doi:10.1016/j.jneumeth.2008.01.027 (2008).
691 15 Avery, L. Motor neuron M3 controls pharyngeal muscle relaxation timing in
692 Caenorhabditis elegans. *J Exp Biol* **175**, 283-297 (1993).

693 16 McKoy, A. F., Chen, J., Schupbach, T. & Hecht, M. H. A novel inhibitor of amyloid
694 beta (Abeta) peptide aggregation: from high throughput screening to efficacy in
695 an animal model of Alzheimer disease. *J Biol Chem* **287**, 38992-39000,
696 doi:10.1074/jbc.M112.348037 (2012).
697 17 Pujols, J. *et al.* High-Throughput Screening Methodology to Identify Alpha-
698 Synuclein Aggregation Inhibitors. *Int J Mol Sci* **18**, doi:10.3390/ijms18030478
699 (2017).
700 18 Kurnik, M. *et al.* Potent alpha-Synuclein Aggregation Inhibitors, Identified by
701 High-Throughput Screening, Mainly Target the Monomeric State. *Cell Chem Biol*
702 **25**, 1389-1402 e1389, doi:10.1016/j.chembiol.2018.08.005 (2018).
703 19 Daina, A., Michielin, O. & Zoete, V. SwissADME: a free web tool to evaluate
704 pharmacokinetics, drug-likeness and medicinal chemistry friendliness of small
705 molecules. *Sci Rep* **7**, 42717, doi:10.1038/srep42717 (2017).
706 20 Burley, S. K. & Petsko, G. A. Aromatic-aromatic interaction: a mechanism of
707 protein structure stabilization. *Science* **229**, 23-28, doi:10.1126/science.3892686
708 (1985).
709 21 Somerville, A. N. SciFinder Scholar. *Journal of Chemical Education* **75**, 959-960,
710 doi:doi.org/10.1021/ed075p959 (1998).
711 22 Ono, M., Haratake, M., Saji, H. & Nakayama, M. Development of novel beta-
712 amyloid probes based on 3,5-diphenyl-1,2,4-oxadiazole. *Bioorg Med Chem* **16**,
713 6867-6872, doi:10.1016/j.bmc.2008.05.054 (2008).
714 23 Watanabe, H. *et al.* Synthesis and biological evaluation of radioiodinated 2,5-
715 diphenyl-1,3,4-oxadiazoles for detecting beta-amyloid plaques in the brain.
716 *Bioorg Med Chem* **17**, 6402-6406, doi:10.1016/j.bmc.2009.07.020 (2009).
717 24 Yang, Y. *et al.* Radioiodinated benzyloxybenzene derivatives: a class of flexible
718 ligands target to beta-amyloid plaques in Alzheimer's brains. *J Med Chem* **57**,
719 6030-6042, doi:10.1021/jm5004396 (2014).
720 25 Geissen, M. *et al.* From high-throughput cell culture screening to mouse model:
721 identification of new inhibitor classes against prion disease. *ChemMedChem* **6**,
722 1928-1937, doi:10.1002/cmdc.201100119 (2011).
723 26 Ayaz, M. *et al.* Flavonoids as Prospective Neuroprotectants and Their
724 Therapeutic Propensity in Aging Associated Neurological Disorders. *Front Aging*
725 *Neurosci* **11**, 155, doi:10.3389/fnagi.2019.00155 (2019).
726 27 Gutierrez-Zepeda, A. *et al.* Soy isoflavone glycitein protects against beta amyloid-
727 induced toxicity and oxidative stress in transgenic Caenorhabditis elegans. *BMC*
728 *Neurosci* **6**, 54, doi:10.1186/1471-2202-6-54 (2005).
729 28 Hirohata, M. *et al.* Anti-amyloidogenic effects of soybean isoflavones in vitro:
730 Fluorescence spectroscopy demonstrating direct binding to Abeta monomers,
731 oligomers and fibrils. *Biochim Biophys Acta* **1822**, 1316-1324,
732 doi:10.1016/j.bbadis.2012.05.006 (2012).
733 29 Bennhold, H. Specific staining of amyloid by Congo red. *Muenchen. Med.*
734 *Wochenschr* **69**, 1537-1538 (1922).
735 30 Divry, P. F., M. Sur les propriétées optiques de l'amyloide. *C. R. Soc. Biol.* **97**,
736 1808-1810 (1927).

31 Vassar, P. S. & Culling, C. F. Fluorescent stains, with special reference to amyloid and connective tissues. *Arch Pathol* **68**, 487-498 (1959).

32 Larbig, G., Pickhardt, M., Lloyd, D. G., Schmidt, B. & Mandelkow, E. Screening for Inhibitors of Tau Protein Aggregation into Alzheimer Paired Helical Filaments: A Ligand Based Approach Results in Successful Scaffold Hopping. *Current Alzheimer Research* **4**, 315-323 (2007).

33 Harrington, B. J. & Raper, K. B. Use of a fluorescent brightener to demonstrate cellulose in the cellular slime molds. *Appl Microbiol* **16**, 106-113 (1968).

34 Baker, L. G., Specht, C. A., Donlin, M. J. & Lodge, J. K. Chitosan, the deacetylated form of chitin, is necessary for cell wall integrity in Cryptococcus neoformans. *Eukaryot Cell* **6**, 855-867, doi:10.1128/EC.00399-06 (2007).

35 Cohen, S. I. *et al.* Proliferation of amyloid-beta42 aggregates occurs through a secondary nucleation mechanism. *Proc Natl Acad Sci U S A* **110**, 9758-9763, doi:10.1073/pnas.1218402110 (2013).

36 Knowles, T. P. *et al.* An analytical solution to the kinetics of breakable filament assembly. *Science* **326**, 1533-1537, doi:10.1126/science.1178250 (2009).

37 Sterling, T. & Irwin, J. J. ZINC 15--Ligand Discovery for Everyone. *J Chem Inf Model* **55**, 2324-2337, doi:10.1021/acs.jcim.5b00559 (2015).

38 Gazit, E. A possible role for pi-stacking in the self-assembly of amyloid fibrils. *FASEB J* **16**, 77-83, doi:10.1096/fj.01-0442hyp (2002).

39 McGaughey, G. B., Gagne, M. & Rappe, A. K. pi-Stacking interactions. Alive and well in proteins. *J Biol Chem* **273**, 15458-15463, doi:10.1074/jbc.273.25.15458 (1998).

40 Caughey, W. S., Raymond, L. D., Horiuchi, M. & Caughey, B. Inhibition of protease-resistant prion protein formation by porphyrins and phthalocyanines. *Proc Natl Acad Sci U S A* **95**, 12117-12122, doi:10.1073/pnas.95.21.12117 (1998).

41 Lee, B. I. *et al.* Photoexcited Porphyrins as a Strong Suppressor of beta-Amyloid Aggregation and Synaptic Toxicity. *Angew Chem Int Ed Engl* **54**, 11472-11476, doi:10.1002/anie.201504310 (2015).

42 Yuan, C. & Gao, Z. Abeta interacts with both the iron center and the porphyrin ring of heme: mechanism of heme's action on Abeta aggregation and disaggregation. *Chem Res Toxicol* **26**, 262-269, doi:10.1021/tx300441e (2013).

43 Panche, A. N., Diwan, A. D. & Chandra, S. R. Flavonoids: an overview. *J Nutr Sci* **5**, e47, doi:10.1017/jns.2016.41 (2016).

44 Akaishi, T. *et al.* Structural requirements for the flavonoid fisetin in inhibiting fibril formation of amyloid beta protein. *Neurosci Lett* **444**, 280-285, doi:10.1016/j.neulet.2008.08.052 (2008).

45 Yin, F. *et al.* Silibinin: a novel inhibitor of Abeta aggregation. *Neurochem Int* **58**, 399-403, doi:10.1016/j.neuint.2010.12.017 (2011).

46 Choi, E. Y., Kang, S. S., Lee, S. K. & Han, B. H. Polyphenolic Biflavonoids Inhibit Amyloid-Beta Fibrillation and Disaggregate Preformed Amyloid-Beta Fibrils. *Biomol Ther (Seoul)* **28**, 145-151, doi:10.4062/biomolther.2019.113 (2020).

47 Kimura, J. *et al.* Nobiletin Reduces Intracellular and Extracellular beta-Amyloid in iPS Cell-Derived Alzheimer's Disease Model Neurons. *Biol Pharm Bull* **41**, 451-457, doi:10.1248/bpb.b17-00364 (2018).

48 Ahmad, A. *et al.* Neuroprotective Effect of Fisetin Against Amyloid-Beta-Induced Cognitive/Synaptic Dysfunction, Neuroinflammation, and Neurodegeneration in Adult Mice. *Mol Neurobiol* **54**, 2269-2285, doi:10.1007/s12035-016-9795-4 (2017).

49 Kim, J. K. *et al.* Protective effects of kaempferol (3,4',5,7-tetrahydroxyflavone) against amyloid beta peptide (Abeta)-induced neurotoxicity in ICR mice. *Biosci Biotechnol Biochem* **74**, 397-401, doi:10.1271/bbb.90585 (2010).

50 Wei, D., Tang, J., Bai, W., Wang, Y. & Zhang, Z. Ameliorative effects of baicalein on an amyloid-beta induced Alzheimer's disease rat model: a proteomics study. *Curr Alzheimer Res* **11**, 869-881 (2014).

51 Chen, C. *et al.* The prodrug of 7,8-dihydroxyflavone development and therapeutic efficacy for treating Alzheimer's disease. *Proc Natl Acad Sci U S A* **115**, 578-583, doi:10.1073/pnas.1718683115 (2018).

52 Wang, L., Zeng, R., Pang, X., Gu, Q. & Tan, W. The mechanisms of flavonoids inhibiting conformational transition of amyloid-b42 monomer: a comparative molecular dynamics simulation study. *RSC Advances* **5**, 66391-66402, doi:DOI: 10.1039/c5ra12328c (2015).

53 Dulovic, A. *et al.* Rhabditophanes diutinus a parthenogenetic clade IV nematode with dauer larvae. *PLoS Pathog* **16**, e1009113, doi:10.1371/journal.ppat.1009113 (2020).

54 Tiwari, O. S. *et al.* Entropically-Driven Co-assembly of l-Histidine and l-Phenylalanine to Form Supramolecular Materials. *ACS Nano* **17**, 3506-3517, doi:10.1021/acsnano.2c09872 (2023).

55 Coelho, A. A. Indexing of powder diffraction patterns by iterative use of singular value decomposition. *J Appl. Cryst.* **36**, 86-95, doi:https://doi.org/10.1107/S0021889802019878 (2003).

56 Altomare, A. *et al.* EXPO2013: a kit of tools for phasing crystal structures from powder data. *J. Appl. Cryst.* **46**, 1231-1235, doi:https://doi.org/10.1107/S0021889813013113 (2013).

57 Toby, B. H. & Von Dreele, R. B. GSAS-II: the genesis of a modern open-source all purpose crystallography software package. *J. Appl. Cryst.* **46**, 544-549, doi:https://doi.org/10.1107/S0021889813003531 (2013).

58 Cline, M. S. *et al.* Integration of biological networks and gene expression data using Cytoscape. *Nat Protoc* **2**, 2366-2382, doi:10.1038/nprot.2007.324 (2007).

59 O'Boyle, N. M. *et al.* Open Babel: An open chemical toolbox. *J Cheminform* **3**, 33, doi:10.1186/1758-2946-3-33 (2011).

60 Schüller, A., Hähnke, V. & Schneider, G. SmiLib v2.0: A Java-Based Tool for Rapid Combinatorial Library Enumeration. *QSAR & Combinatorial Science* **3**, 407-410 (2007).

821 61 Habchi, J. *et al.* Systematic development of small molecules to inhibit specific
822 microscopic steps of Abeta42 aggregation in Alzheimer's disease. *Proc Natl Acad*
823 *Sci U S A* **114**, E200-E208, doi:10.1073/pnas.1615613114 (2017).
824

825 **Figure 1. Crystal-Forming Small Molecules are Compact and Aromatic. A.** A schematic
826 of *C. elegans* anatomy (from WormAtlas; used with permission). The pharynx is green.
827 **B & C.** Anterior-most region of a worm expressing the IDPC-1::GFP cuticle marker [9]
828 treated with either 1% DMSO solvent control (B) or 30 μM wact-190 (C) for six hours.
829 Orange arrows indicate the buccal cavity cuticle, the green arrows highlight the buccal
830 collar, the white arrows indicate the cuticle that lines the channels, and the blue
831 arrowheads highlight the birefringent crystals. Differential interference contrast (DIC),
832 birefringent (BIRE), and the IDPC-1::GFP (cuticle) images are shown. The scale bar in B
833 applies to all images in the upper right-hand side. **D.** Crystalizing molecules have
834 significantly fewer rotatable bonds and hydrogen-bond donors, but greater aromaticity,
835 and compactness (as measured by van der Waals volume and fraction Csp3) compared
836 to non-crystalizing molecules from the same library. The mean and standard error is
837 shown.

838 **Figure 2. Biophysical Analyses of *in vitro* Small Molecule Crystals. A.** The chemical
839 structure of wact-190. **B.** The unit cell with wact-190 molecules whose centroid lies
840 within the unit cell with the three coordinates shown with white letters and black
841 corresponding arrows. The wact-190 crystal unit cell shows two molecules per
842 asymmetric unit cell in a triclinic and anti-parallel packing arrangement. **C.** The 3D
843 crystal packing arrangement along the b-axis (see Supplemental Figure 2a-2c for other
844 aspects). **D.** The calculated distance between the indicated centroid (pink sphere) of two
845 adjacent molecules stacked along crystallographic b-axis within the wact-190 crystal is
846 approximately 5.0 Å. **E.** The experimental and simulated PXRD patterns of wact-190
847 molecule (see Supplemental Figure 2d for more details). **F.** The chemical structure of
848 wact-416. **G.** The unit cell with wact-416 molecules whose centroid lies within the
849 crystal unit cell. The wact-416 crystal unit cell shows four molecules per asymmetric unit
850 cell in an orthorhombic and parallel packing arrangement. **H.** The 3D crystal packing
851 (view along crystallographic b-axis) shows parallel packing for wac-416 crystals (see
852 Supplemental Figure 2e-2g for other aspects). **I.** The calculated distance between the
853 indicated centroid (pink sphere) of the 6-membered rings of two adjacent molecules
854 stacked along crystallographic b-axis within the wact-416 crystal is approximately 4.9 Å.
855 **J.** The experimental and simulated PXRD patterns of wact-416 molecule (see
856 Supplemental Figure 2h for more details).

857 **Figure 3. A Structural Similarity Network of 65 Crystal-Forming Compounds. A.** An
858 unsupervised structural similarity network of the 65 crystalizing molecules. Each node
859 represents a small molecule, labelled with a wactive number or DHV (dehydrovariabilin).
860 The link represents a Tanimoto score of structural similarity of the core scaffold of 0.8 or
861 higher. The lower-case labels indicate groups of molecules with the same core scaffolds
862 as indicated in B. Nodes highlighted in pink indicate a core scaffold known to interact
863 with amyloids (see Supplemental Table 3 and Supplemental Data File 1 for details). The
864 asterisks on the wact-128 node highlights that visual inspection reveals that it is a
865 distinct scaffold despite its connection to wact-381 and represents the 30th unique
866 family. **B.** Markush representations of the core scaffolds of structural analogs able to
867 crystalize in the worm. R, X, and Y groups are shown in Supplemental Figure 1.

868 **Figure 4. Crystals Preferentially Disrupt Amyloid Dye-Staining Material of the**
869 **Pharyngeal Cuticle. A-F.** Images of the anterior-most end of the worm**.** The imaging
870 channel is indicated (lower left) as is the wactive treatment (left-hand side of
871 micrograph series). DIC, differential interference contrast; bire, birefringence; CFW,
872 calcofluor white; ThS, thioflavin S; EY, eosin Y. Merge 1 is the merge of the two dye
873 signals. Merge 2 is the merge of the signals from the amyloid-binding dye and
874 birefringence. Blue arrows indicate overlapping signals of the amyloid-binding dye and
875 birefringence; orange arrows show a lack of amyloid-binding dye signal associated with
876 birefringence signal. The scale in A applies to A-F. **G.** Control for the ability of dyes to
877 bind wactive crystals. Precipitate of wact-190 or wact-390 was formed in solution (or
878 DMSO solvent control) and was subsequently stained with the dye indicated on the right
879 of each set. The dyes were used at the same concentration as the *in vivo* staining
880 experiments as described in the methods. Each condition was imaged using DIC,
881 birefringence (bire.) or the appropriate fluorescent (floures.) channel, as indicated on
882 the left of each panel. The dyes were not rinsed from the slide, which accounts for the
883 non-specific signal in the EY fluorescent channel. The scale in the upper left micrograph
884 applies to all images in G. **H-I.** Controls for the fluorescence of crystals in the different
885 channels. D, differential interference contrast (DIC); B, birefringence; C, CFP; G, GFP; Y,
886 YFP; R, RFP channels. The scale bar in H also applies to I. 60 μM of wact-190 and wact-
887 390 was used in all experiments relevant to panels A-I.

888 **Figure 5. Amyloid-Binding Dyes Suppress Crystal Formation. A.** Six-day viability assay
889 results illustrating that amyloid binding dyes (CR and ThS) can suppress wact-190-
890 induced lethality, but that chitin/chitosan-binding dyes (CFW and EY) cannot. Each cell
891 shows the summary of 3 trials each done in quadruplicate. **B-C.** Amyloid-binding dyes,
892 but not chitin/chitosan-binding dyes, can suppress crystal formation. On the top row,
893 animals were pre-incubated in the indicated dye or solvent control for 3 hours. Then,
894 the right-most five samples were incubated in 60 μM wact-190 for three hours without
895 the initial dyes present. On the bottom row of (B), animals were incubated in the
896 indicated dye or solvent control, and for the five right-most five samples, simultaneously
897 incubated with wact-190 (60 μM) for 3 hours. Representative birefringence images are
898 shown in (B) and the corresponding signal quantification is reported in (C). The scale bar
899 in the upper left of B applies to all images in the series. Samples labelled with an asterisk
900 indicates a significant difference relative to control (p<0.01). Standard error of the mean
901 is shown.

902 **Figure 6. Aβ42 Fibrils can Seed wact-190 Objects.** Transmission electron microscopy
903 (TEM) images of solutions allowed to self-assemble overnight. **A-D.** Mixing solutions of
904 25 μM Aβ42 and 25 μM wact-190 in PBS. Unmixed 25 μM Aβ42 (A) and 25 μM wact-190
905 (B); 1-fold Aβ42 diluted with 2-fold wact-190 (to a final concentration of 8.33 μM Aβ42
906 and 16.66 μM wact-190) (C); 1-fold Aβ42 and 10-fold wact-190 (to a final concentration
907 of 2.27 μM Aβ42 and 22.72 μM wact-190) (D). **E-H.** Mixing solutions of 25 μM Aβ42 and
908 0.5 μM wact-190 in PBS. Unmixed 25 μM Aβ42 (E) and 0.5 μM wact-190 (F); 1-fold Aβ42
909 diluted with 1-fold wact-190 (to a final concentration of 12.5 μM Aβ42 and 0.25 μM
910 wact-190)(G and H). **I-L.** Mixing solutions of 25 μM Aβ42 and 0.1 μM wact-190 in PBS.
911 Unmixed 25 μM Aβ-42 (I) and 0.1 μM wact-190 (J); 1-fold Aβ42 diluted with 1-fold wact-
912 190 (to a final concentration of 12.5 μM Aβ42 and 0.05 μM wact-190) (K and L).
913 Examples of Aβ42 amyloid fibrils are indicated with a blue arrow and examples of
914 presumptive wact-190 objects that are associated with Aβ42 fibrils are indicated with a
915 red arrow.

916 **Figure 7. A Screen for wact-190 Suppressors Reveals Amyloid-Disrupting Molecules. A.**
917 A structural similarity network of the 85 Spectrum library hits that suppress wact-190
918 lethality and crystal formation. The nodes (circles) represent a drug or natural product.
919 The links (straight lines) represent a Tanimoto score of structural similarity of 0.8 or
920 more (see Methods). A bold red outline indicates known disruptors of amyloid fibril
921 formation. See Supplementary Table 3 for details and names of the compounds. **B.** Core
922 scaffolds among the drug suppressors of crystal formation. The small case letter
923 preceding the scaffold name corresponds to the nodes indicated in (A). The number (n)
924 of individual molecules within the network is indicated, as is the enrichment of that
925 scaffold within the network relative to that expected by random chance based on the
926 prevalence of that scaffold within the entire library (the hypergeometric *p* value is
927 shown). The benzaldehyde substructure is highlighted in blue. **C.** Examples of the
928 localization of crystal suppressors (60 μM) that are fluorescent. Calcofluor white (CFW)
929 is used as a counter-stain control; curcu., curcumin; harmal., harmaline; erythro.,
930 erythrosine. See Supplemental Figure 5 for additional examples and controls. The scale
931 in panel C applies to all images in the series. **D-H.** *In vitro* assays to characterize the
932 ability of the indicated molecule to inhibit Aβ42 fibril formation in secondary nucleation
933 assays (see methods, Supplementary Table 5 and Supplementary Figure 8 for additional
934 details). Adapalene is a known standard inhibitor of Aβ42 fibril formation [61].

935 **Figure 8. Crystallizers and Suppressors can Share Identical Core Structures. A-C.**
936 Physicochemical features of crystallizers and suppressors. A single and double asterisk
937 indicate $p<0.001$ and $p<1.0E-10$, respectively. The standard error of the mean is shown.
938 **D.** Crystallizers and suppressors sharing an identical or similar core structure. **E.** Core
939 scaffolds of suppressing molecules that can be turned into crystallizers (see
940 Supplemental Table 6 for additional details). **F.** Core scaffolds of crystallizing molecules
941 that can be turned into suppressors (see Supplemental Table 7 for additional details). **G.**
942 *In vitro* assays to characterize the ability of the indicated suppressor molecule to inhibit
943 Aβ42 fibril formation in secondary nucleation assays (see methods and Supplementary
944 Figure 8 for additional details).

Figure 1

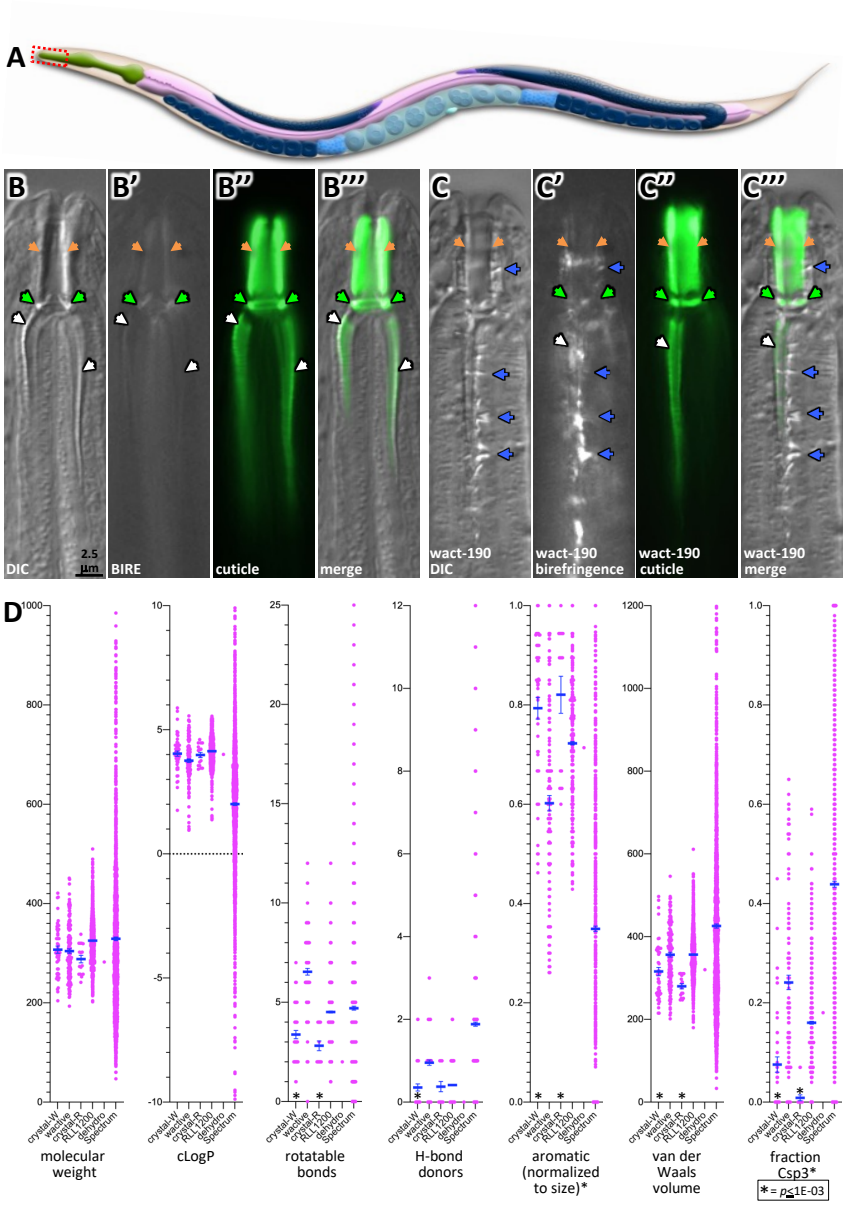
A
B
B'
B''
B'''
C
C'
C''
C'''
DIC
2.5 µm
BIRE
cuticle
merge
wact-190 DIC
wact-190 birefringence
wact-190 cuticle
wact-190 merge
D
crystal-W
wactive
crystal-R
RLL1200
dehydro
Spectrum
molecular weight
cLogP
rotatable bonds
H-bond donors
aromatic (normalized to size)*
van der Waals volume
fraction Csp3*
* = p≤1E-03

Figure 2

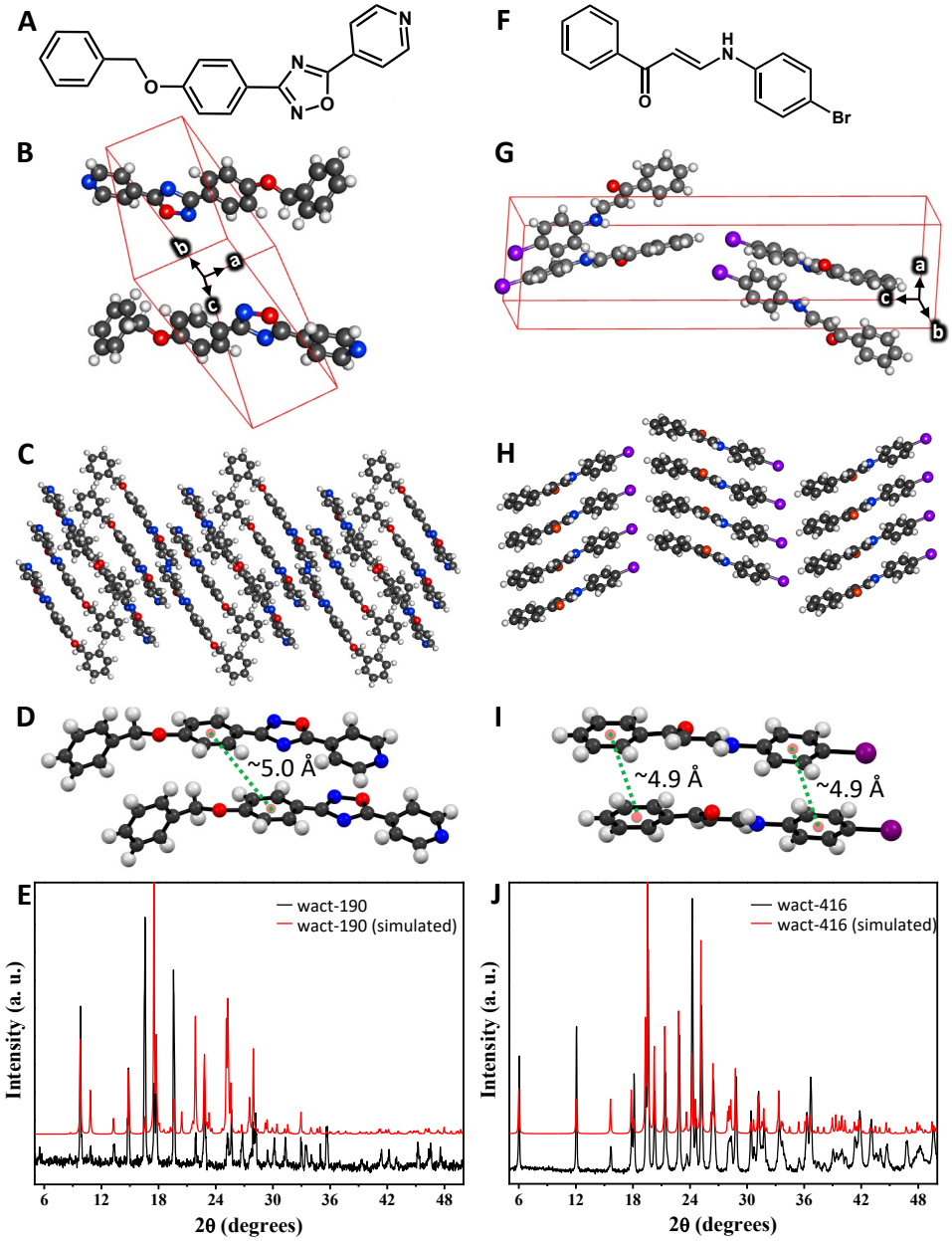
A
F
B
G
C
H
D
~5.0 Å
I
~4.9 Å
~4.9 Å
E
wact-190
wact-190 (simulated)
Intensity (a. u.)
2θ (degrees)
J
wact-416
wact-416 (simulated)
Intensity (a. u.)
2θ (degrees)

Figure 3

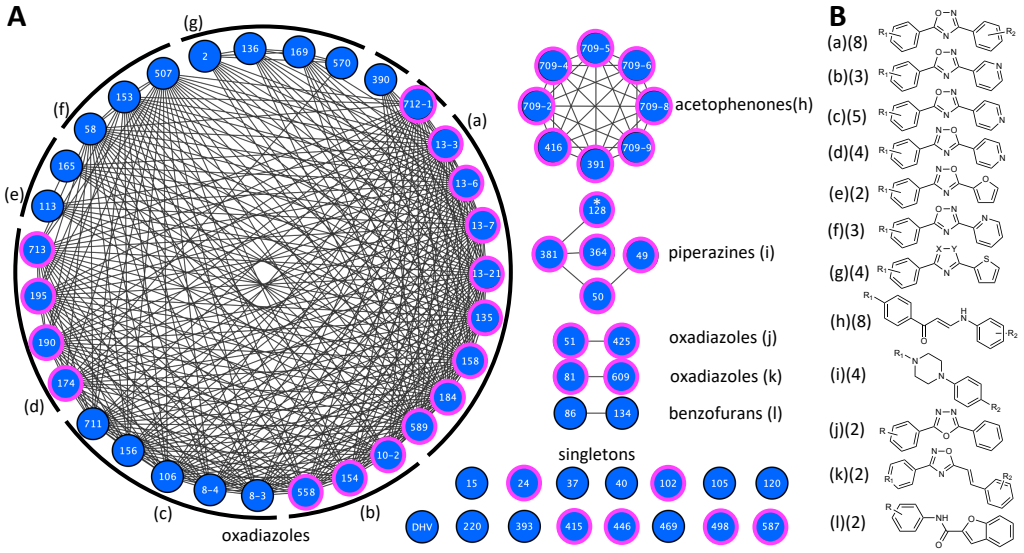
A
(g)
(f)
(e)
(d)
(c)
(b)
(a)
oxadiazoles
acetophenones(h)
piperazines (i)
oxadiazoles (j)
oxadiazoles (k)
benzofurans (l)
singletons
B
(a)(8)
(b)(3)
(c)(5)
(d)(4)
(e)(2)
(f)(3)
(g)(4)
(h)(8)
(i)(4)
(j)(2)
(k)(2)
(l)(2)

Figure 4

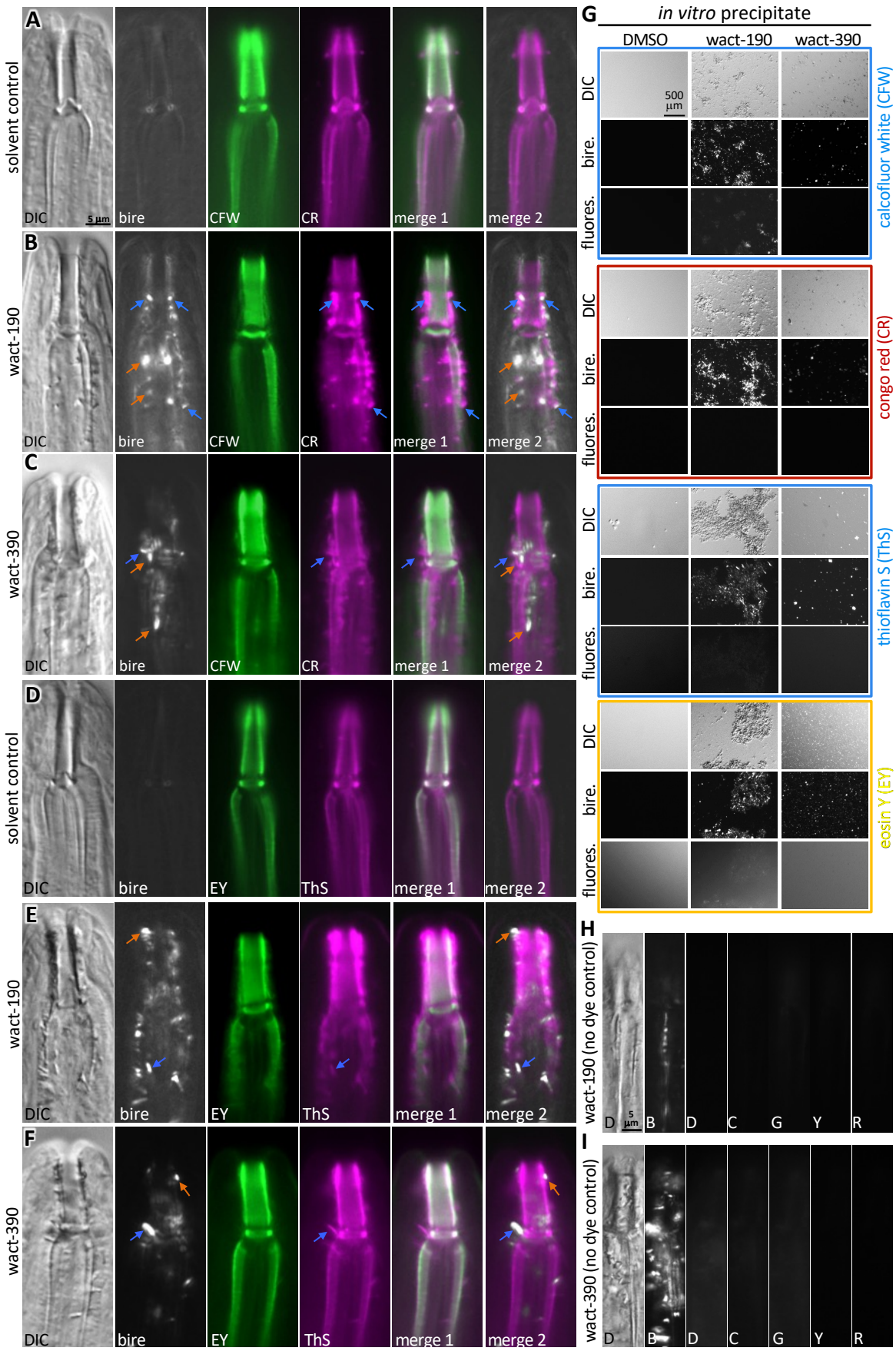
A
solvent control
DIC
5 µm
bire
CFW
CR
merge 1
merge 2
B
wact-190
C
wact-390
D
EY
ThS
E
F
G
in vitro precipitate
DMSO
wact-190
wact-390
500 µm
fluores.
calcofluor white (CFW)
congo red (CR)
thioflavin S (ThS)
eosin Y (EY)
H
wact-190 (no dye control)
D
B
C
G
Y
R
I
wact-390 (no dye control)

Figure 5

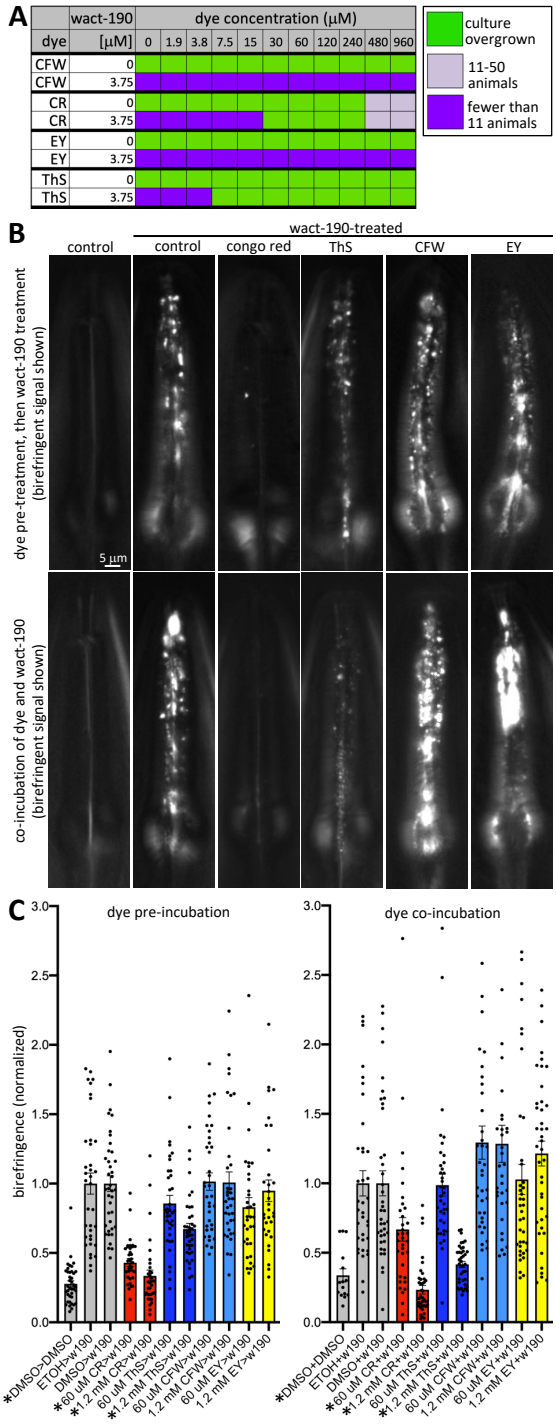
A
wact-190
dye concentration (μM)
dye
[μM]
0
1.9
3.8
7.5
15
30
60
120
240
480
960
CFW 0
CFW 3.75
CR 0
CR 3.75
EY 0
EY 3.75
ThS 0
ThS 3.75
culture overgrown
11-50 animals
fewer than 11 animals
B
wact-190-treated
control
control
congo red
ThS
CFW
EY
dye pre-treatment, then wact-190 treatment (birefringent signal shown)
co-incubation of dye and wact-190 (birefringent signal shown)
5 μm
C
dye pre-incubation
dye co-incubation
birefringence (normalized)
3.0
2.5
2.0
1.5
1.0
0.5
0.0
*DMSO>DMSO
ETOH>w190
DMSO>w190
*60 uM CR>w190
*1.2 mM CR>w190
60 uM ThS>w190
*1.2 mM ThS>w190
60 uM CFW>w190
1.2 mM CFW>w190
60 uM EY>w190
1.2 mM EY>w190
*DMSO+DMSO
ETOH+w190
DMSO+w190
*60 uM CR+w190
*1.2 mM CR+w190
60 uM ThS+w190
*1.2 mM ThS+w190
60 uM CFW+w190
1.2 mM CFW+w190
60 uM EY+w190
1.2 mM EY+w190

Figure 6

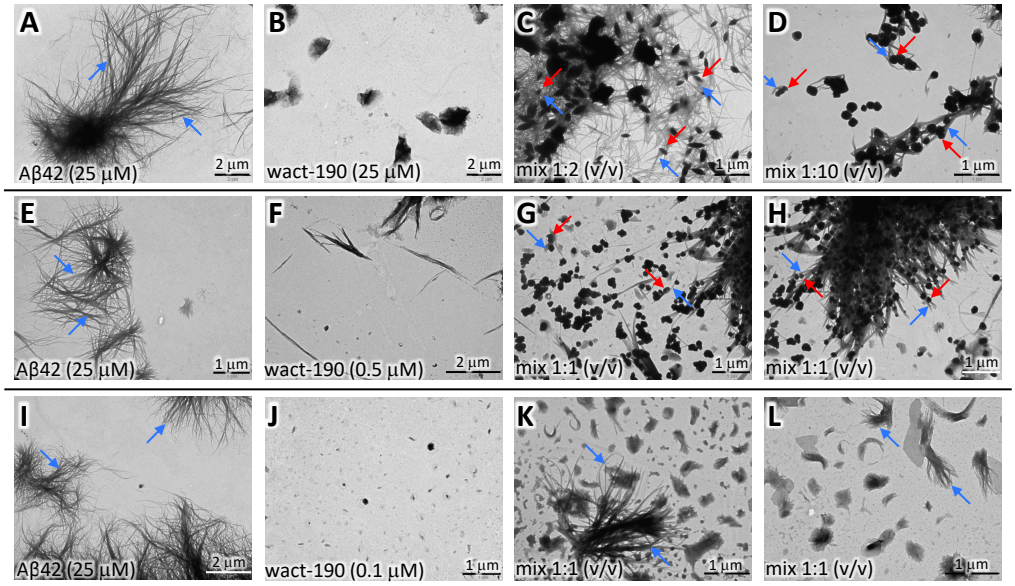
A
Aβ42 (25 μM)
2 μm
B
wact-190 (25 μM)
2 μm
C
mix 1:2 (v/v)
1 μm
D
mix 1:10 (v/v)
1 μm
E
Aβ42 (25 μM)
1 μm
F
wact-190 (0.5 μM)
2 μm
G
mix 1:1 (v/v)
1 μm
H
mix 1:1 (v/v)
1 μm
I
Aβ42 (25 μM)
2 μm
J
wact-190 (0.1 μM)
1 μm
K
mix 1:1 (v/v)
1 μm
L
mix 1:1 (v/v)
1 μm

Figure 7

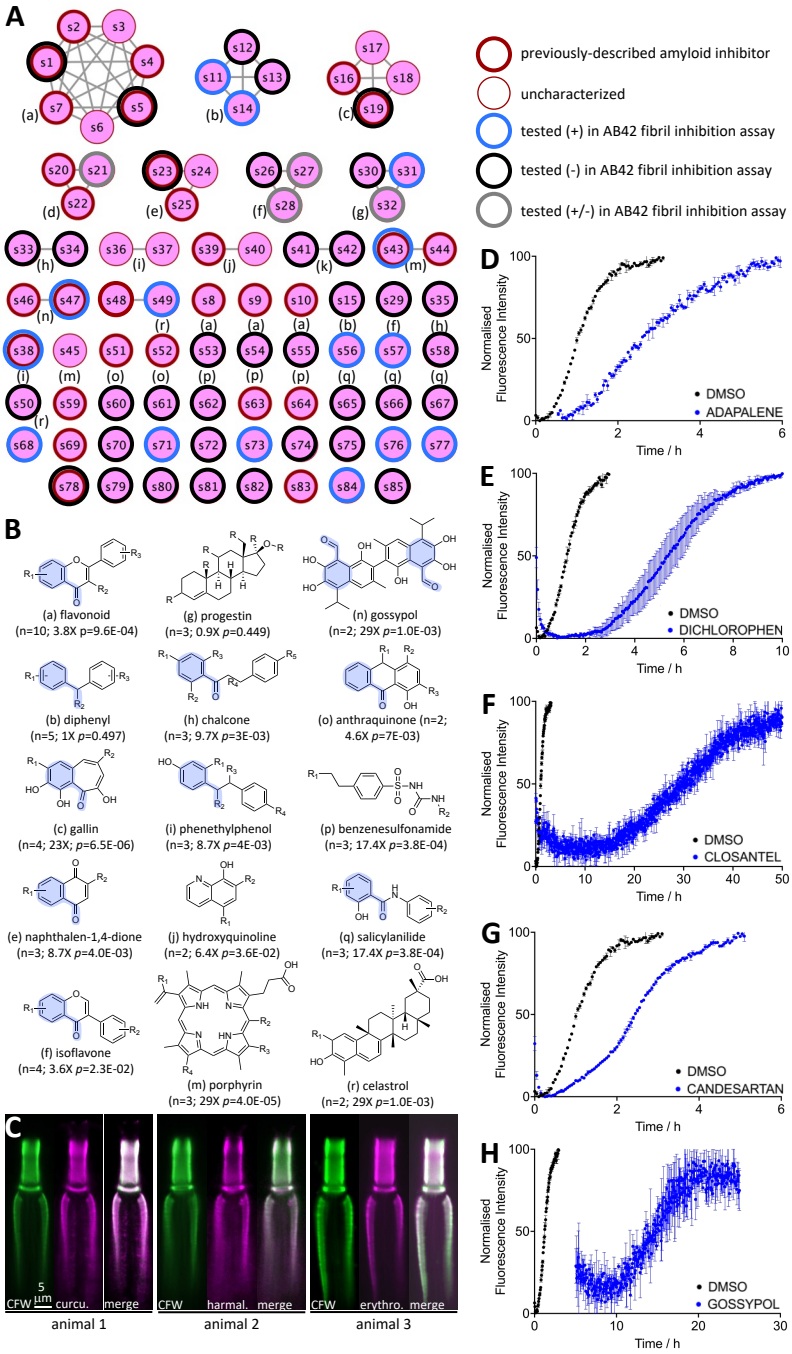
A
B
C
previously-described amyloid inhibitor
uncharacterized
tested (+) in AB42 fibril inhibition assay
tested (-) in AB42 fibril inhibition assay
tested (+/-) in AB42 fibril inhibition assay
(a) flavonoid (n=10; 3.8X p=9.6E-04)
(g) progestin (n=3; 0.9X p=0.449)
(n) gossypol (n=2; 29X p=1.0E-03)
(b) diphenyl (n=5; 1X p=0.497)
(h) chalcone (n=3; 9.7X p=3E-03)
(o) anthraquinone (n=2; 4.6X p=7E-03)
(c) gallin (n=4; 23X; p=6.5E-06)
(i) phenethylphenol (n=3; 8.7X p=4E-03)
(p) benzenesulfonamide (n=3; 17.4X p=3.8E-04)
(e) naphthalen-1,4-dione (n=3; 8.7X p=4.0E-03)
(j) hydroxyquinoline (n=2; 6.4X p=3.6E-02)
(q) salicylanilide (n=3; 17.4X p=3.8E-04)
(f) isoflavone (n=4; 3.6X p=2.3E-02)
(m) porphyrin (n=3; 29X p=4.0E-05)
(r) celastrol (n=2; 29X p=1.0E-03)
CFW curcu. merge
CFW harmal. merge
CFW erythro. merge
5 µm
animal 1
animal 2
animal 3
D
E
F
G
H
Normalised Fluorescence Intensity
Time / h
DMSO
ADAPALENE
DICHLOROPHEN
CLOSANTEL
CANDESARTAN
GOSSYPOL

Figure 8

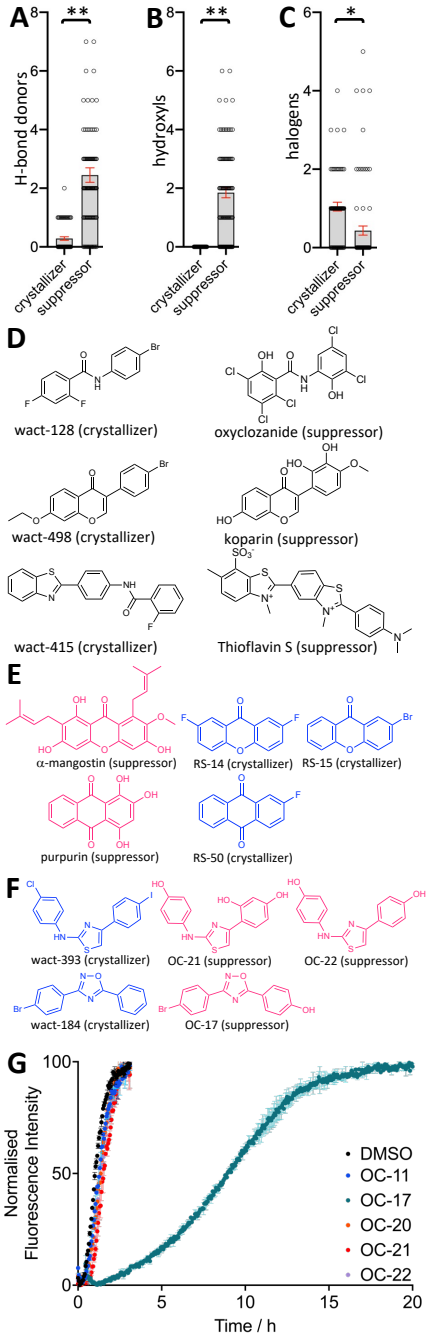
A
B
C
H-bond donors
hydroxyls
halogens
crystallizer
suppressor
D
wact-128 (crystallizer)
oxyclozanide (suppressor)
wact-498 (crystallizer)
koparin (suppressor)
wact-415 (crystallizer)
Thioflavin S (suppressor)
E
α-mangostin (suppressor)
RS-14 (crystallizer)
RS-15 (crystallizer)
purpurin (suppressor)
RS-50 (crystallizer)
F
wact-393 (crystallizer)
OC-21 (suppressor)
OC-22 (suppressor)
wact-184 (crystallizer)
OC-17 (suppressor)
G
Normalised Fluorescence Intensity
Time / h
DMSO
OC-11
OC-17
OC-20
OC-21
OC-22

Supplemental Table 1

	source	wactive crystal (avg)	wactive no-crystal (avg)	wactive ttest	RLL1200 crystal (avg)	RLL1200 no-crystal (avg)	RLL1200 ttest	wact v RLL crystallizer ttest	Spectrum dehydrovariabili	Spectrum no-crystal (avg)
Size Features										
molecular weight	Open Babel	307.16	304.30	7.5E-01	288.09	324.67	2.3E-03	1.6E-01	282.29	328.75
molar refractivity	Open Babel	82.05	84.59	3.2E-01	73.28	87.32	5.8E-06	2.9E-02	79.17	88.36
van der Walls volume	Open Babel	315.72	356.40	7.3E-04	280.14	356.26	2.6E-07	5.4E-02	320.08	424.60
Hydrogen Bonding Features										
hydrogen bond acceptors (method 1)	Open Babel	2.96	2.53	3.3E-02	2.44	3.79	6.8E-05	4.9E-02	3.00	5.13
hydrogen bond acceptors (method 2)	Open Babel	3.73	2.82	4.6E-05	3.06	4.62	2.8E-04	5.5E-02	4.00	5.40
hydrogen bond donors	Open Babel	0.35	0.95	2.4E-06	0.38	0.41	8.0E-01	9.0E-01	0.00	1.93
number of OH at pH 7.4	Open Babel	0.02	0.04	5.3E-01	0.00	0.00	8.4E-01	5.7E-01	0.00	1.03
Bond (non-aromatic) Features										
bonds	Open Babel	22.90	21.85	1.2E-01	20.44	24.18	2.0E-05	2.2E-02	24.00	24.50
aromatic bonds	Open Babel	16.54	12.26	2.6E-10	15.44	16.08	4.1E-01	2.8E-01	16.00	7.66
single bonds	Open Babel	5.73	8.83	4.3E-06	4.25	7.49	7.7E-07	7.7E-02	8.00	14.89
double bonds	Open Babel	0.63	0.74	4.0E-01	0.75	0.53	2.1E-01	6.3E-01	0.00	1.92
triple bonds	Open Babel	0.00	0.02	3.2E-01	0.00	0.08	2.6E-01	n/a	0.00	0.03
rotatable bonds	Open Babel	3.38	4.54	4.3E-05	2.81	4.50	6.6E-05	9.7E-02	2.00	4.70
Atom Features										
number of heavy atoms	Open Babel	20.79	20.30	4.0E-01	18.75	22.20	1.1E-05	3.0E-02	21.00	22.89
number of H	Open Babel	12.06	16.32	9.1E-07	9.81	14.65	1.1E-06	5.9E-02	14.00	21.18
number of C	Open Babel	15.75	15.64	8.2E-01	14.38	16.69	2.7E-04	1.0E-01	17.00	16.88
number of N	Open Babel	2.27	1.94	3.9E-02	2.00	2.51	1.4E-02	2.8E-01	0.00	1.50
number of O	Open Babel	1.65	1.36	7.0E-02	1.06	1.78	5.2E-03	1.4E-02	4.00	3.97
number of S	Open Babel	0.21	0.27	4.4E-01	0.00	0.40	3.7E-03	7.6E-02	0.00	0.20
number of P	Open Babel	0.00	0.00	na	0.00	0.00	na	na	0.00	0.02
number of F	Open Babel	0.33	0.37	8.1E-01	0.50	0.24	1.0E-01	3.8E-01	0.00	0.10
number of Cl	Open Babel	0.31	0.55	4.8E-02	0.31	0.42	5.3E-01	1.0E+00	0.00	0.15
number of Br	Open Babel	0.23	0.11	4.7E-02	0.50	0.17	4.1E-04	4.1E-02	0.00	0.01
number of I	Open Babel	0.04	0.05	7.4E-01	0.00	0.01	7.8E-01	4.1E-01	0.00	0.03
number of B	Open Babel	0.00	0.00		0.00	0.00	na	na	0.00	0.00
number of As	Open Babel	0.00	0.00		0.00	0.00	na	na	0.00	0.00
number of Si	Open Babel	0.00	0.00		0.00	0.00	na	na	0.00	0.00
number of Se	Open Babel	0.00	0.00		0.00	0.00	na	na	0.00	0.00
number of Te	Open Babel	0.00	0.00		0.00	0.00	na	na	0.00	0.00
number of halogens	Open Babel	0.92	1.09	3.6E-01	1.31	0.82	3.2E-02	1.3E-01	0.00	0.29
halides as a percentage of MW	Open Babel	0.13	0.13	9.5E-01	0.20	0.10	8.0E-05	5.2E-02	0.00	0.03
Aromaticity Features										
number of rings	Open Babel	3.10	2.56	2.1E-05	2.69	2.98	4.9E-02	2.9E-02	4.00	2.61
aromatic rings	Open Babel	2.94	2.15	1.1E-09	2.69	2.84	3.2E-01	2.0E-01	3.00	1.35
non-aromatic rings	Open Babel	0.17	0.41	1.1E-02	0.00	0.14	1.2E-01	1.3E-01	1.00	1.26
fraction of atoms in aromatic rings	Open Babel	0.79	0.60	1.3E-09	0.82	0.72	1.1E-03	5.4E-01	0.71	0.35
fraction of aromatic rings over total rings	Open Babel	0.95	0.86	3.0E-03	1.00	0.96	1.2E-01	1.2E-01	0.75	0.56
number of aromatic heavy atoms	SwissADME	16.33	12.05	4.3E-11	15.38	15.97	4.3E-01	3.4E-01	15.00	7.39
fraction Csp3	SwissADME	0.08	0.24	5.5E-09	0.01	0.16	3.4E-09	1.7E-02	0.18	0.44
Charge Features										
number of (+) charges at pH 7.4	Open Babel	0.15	0.52	1.8E-04	0.00	0.06	3.0E-01	1.1E-01	0.00	0.41
number of (-) charges at pH 7.4	Open Babel	0.10	0.09	7.3E-01	0.00	0.00	na	1.8E-01	1.00	0.35
net charge at pH 7.4	Open Babel	0.04	0.44	1.7E-05	0.00	0.06	3.0E-01	4.1E-01	-1.00	0.06
number of aliphatic primary amines	Open Babel	0.00	0.01	5.7E-01	0.00	0.00	na	na	0.00	0.09
number of aliphatic secondary amines	Open Babel	0.00	0.15	4.6E-03	0.00	0.00	na	na	0.00	0.06
number of aliphatic tertiary amines	Open Babel	0.02	0.25	1.0E-03	0.00	0.06	3.3E-01	5.7E-01	0.00	0.16
number of aliphatic amines	Open Babel	0.02	0.40	2.3E-05	0.00	0.06	3.3E-01	5.7E-01	0.00	0.32
number of COOH/COO-	Open Babel	0.00	0.00	na	0.00	0.00	na	na	0.00	0.23
Solubility Features										
LogP	Open Babel	4.04	3.76	5.0E-02	3.99	4.14	3.2E-01	7.8E-01	4.01	2.55
iLogP	SwissADME	2.99	3.05	4.7E-01	2.96	3.22	2.3E-02	7.4E-01	3.29	2.22
XLogP3	SwissADME	3.77	3.72	6.9E-01	3.94	3.93	9.5E-01	4.1E-01	3.47	2.08
WLogP	SwissADME	3.95	3.58	1.7E-02	4.10	4.01	6.0E-01	5.2E-01	3.86	2.16
MLogP	SwissADME	2.75	2.95	1.3E-01	3.04	2.68	6.9E-02	2.0E-01	1.95	1.31
LogP (Silicos-IT)	SwissADME	3.77	3.71	7.3E-01	3.93	4.12	2.4E-01	6.1E-01	4.01	2.21
Consensus LogP	SwissADME	3.45	3.40	6.8E-01	3.59	3.59	9.9E-01	4.4E-01	3.32	1.99
LogS	Open Babel	-5.13	-5.01	4.2E-01	-5.05	-5.61	5.1E-03	7.8E-01	-5.16	-3.24
LogS (Ali)	SwissADME	-4.62	-4.38	6.0E-02	-4.49	-4.99	1.3E-02	7.7E-01	-4.01	-3.46
LogS (Silicos-IT)	SwissADME	-6.37	-5.82	5.0E-03	-6.31	-6.72	7.1E-02	8.7E-01	-6.07	-3.71
LogS (ESOL)	SwissADME	-4.48	-4.22	8.9E-03	-4.53	-4.57	8.1E-01	3.7E-01	-4.17	-3.10
Drug-Like Features										
leadlikeness (# of violations)	SwissADME	1.02	1.02	9.9E-01	0.69	1.05	5.3E-02	7.1E-02	0.00	1.12
Lipinski Drug Prediction (# of violations)	SwissADME	0.06	0.07	9.1E-01	0.06	0.03	4.7E-01	1.0E+00	0.00	0.29
Ghose Drug Prediction (# of violations)	SwissADME	0.02	0.03	8.2E-01	0.00	0.02	5.9E-01	5.7E-01	0.00	0.79
Veber Drug Prediction (# of violations)	SwissADME	0.00	0.00	na	0.00	0.01	7.0E-01	na	0.00	0.19
Egan Drug Prediction (# of violations)	SwissADME	0.00	0.01	4.2E-01	0.00	0.03	4.9E-01	na	0.00	0.19
Muegge Drug Prediction (# of violations)	SwissADME	0.04	0.03	7.9E-01	0.00	0.08	2.6E-01	4.1E-01	0.00	0.75
bioavailability score	SwissADME	0.55	0.55	1.6E-14	0.55	0.55	9.1E-01	2.8E-06	0.55	0.53
PAINS (# of alerts)	SwissADME	0.10	0.12	7.7E-01	0.00	0.01	7.7E-01	1.8E-01	0.00	0.09
Brenk (# of alerts)	SwissADME	0.42	0.58	3.2E-01	0.38	0.11	1.4E-02	8.6E-01	0.00	0.62
log Kp (cm/s) (skin permeation)	SwissADME	-5.50	-5.51	8.7E-01	-5.26	-5.49	7.8E-02	6.9E-02	-5.56	-6.78
synthetic accessibility	SwissADME	2.74	2.48	1.7E-03	2.56	2.89	1.1E-03	9.2E-02	3.42	3.46
Miscellaneous Features										
melting point	Open Babel	148.97	135.06	3.6E-02	138.46	152.54	1.1E-01	3.1E-01	131.56	169.94
topological polar surface area	Open Babel	55.14	46.89	1.8E-02	40.65	64.70	6.2E-04	6.4E-03	40.83	85.95
BBB permeant (1=yes; 0=no)	SwissADME	0.83	0.87	5.0E-01	1.00	0.66	4.3E-03	8.3E-02	1.00	0.45
MDR1 substrate	SwissADME	0.08	0.15	2.2E-01	0.00	0.05	3.5E-01	2.4E-01	1.00	0.31

Compound	**Wact-190**	**Wact-416**
CCDC number	2281946	2282440
Crystal description	White crystalline powder	White crystalline powder
Diffractometer	Bruker D8 DISCOVER	Bruker D8 DISCOVER
Temperature (K)	298	298
Chemical Formula	$C_{20}H_{15}N_3O_2$	$C_{15}H_{12}BrNO$
Formula weight (g/mol)	329.35	302.16
Wavelength	1.54050	1.54050
z	2	4
Crystal System	Triclinic	Orthorhombic
Space group	P-1	$Pna2_1$
a(Å)	5.004(2)	7.58957(25)
b(Å)	10.662(5)	5.77111(20)
c(Å)	16.651(18)	29.4038(15)
α(°)	91.89(5)	90
β(°)	104.029(18)	90
γ(°)	107.259(3)	90
Volume(Å^3)	817.9(3)	1287.89(6)
P(g/cm^3)	1.337	1.558
μ(mm^{-1})	0.718	4.234
F(000)	344.0	608.0
2θ range(°)	5-70	5-70
Index max	h=3,k=7,l=12	5,4,21
N. reflections	712	285
n. parameters	98	33
R_{wp}, GOF on the pattern	4.65%, 1.6	4.74%, 1.4
R_F, R_{F^2}	9.69, 9.62	4.90, 7.14

Supplemental Table 2. Crystallographic data collection and refinement statistics data for the crystal of wact-190 and wact-416.

Supplemental Table 3

#	scaffold[a]	trivial name	Chembridge ID[b]	crystals[c] %	sd	N	Structure[d]	Common Substructure[d] (aka Core Scaffold)	SciFinder Scholar Substructure[e]	PMID/Patent (2022-04)[f]
1	a	wact-13-3	5690016	52	9	2	n1c(noc1c1cc(OC)ccc1)c1ccccc1	c1(c2ccccc2)noc(c3ccccc3)n1	*2250 analogs, 127 refs	18550375, 23766818; US20110081297;
2	a	wact-13-6	5910375	100	0	2	n1c(noc1c1ccc(cc1)Br)c1ccccc1			
3	a	wact-13-7	6141272	100	0	2	n1c(noc1c1ccc(cc1)Br)c1ccc(cc1)F			
4	a	wact-13-21	7530844	100	0	2	n1c(c2c(F)cccc2)onc1c1ccc(cc1)Cl			
5	a	wact-135	7986793	47	40	8	n1c(noc1c1ccccc1)c1cc(OC)ccc1			
6	a	wact-158	9017109	99	2	4	n1c(noc1c1ccc(cc1)F)c1cc(Br)ccc1			
7	a	wact-184	9034543	100	1	4	n1c(noc1c1ccccc1)c1ccc(cc1)Br			
8	a	wact-589	5229759	88	5	3	n1c(noc1c1ccccc1)c1ccccc1			
9	b	wact-10-2	6033348	98	3	2	n1c(noc1c1ccc(cc1)Br)c1cnccc1	c1(c2cccnc2)noc(c3ccccc3)n1	2431 analogs, 353 refs	US20110081297
10	b	wact-154	9013615	34	12	4	n1c(noc1c1ccc(OCc2ccccc2)cc1)c1cnccc1			
11	b	wact-558	9008591	29	15	4	n1c(noc1c1ccc(OCC(C)C)cc1)c1cnccc1			
12	c	wact-8-3	5905759	100	0	2	n1c(noc1c1ccc(cc1)Br)c1ccncc1	c1(c2ccncc2)noc(c3ccccc3)n1	1309 analogs, 101 refs, 0 amy.ints	
13	c	wact-8-4	6715898	49	10	2	n1c(noc1c1cc(c(cc1)C)Cl)c1ccncc1			
14	c	wact-106	7783279	81	22	5	n1c(c2c(ccc(c2)Br)Cl)onc1c1ccncc1			
15	c	wact-156	9016428	71	20	6	n1c(c2c(cc(c(c2)F)F)Cl)onc1c1ccncc1			
16	c	wact-711	6945665	43	17	2	n1c(noc1c1cc2c(cc1)cccc2)c1ccncc1			
17	d	wact-174	9026631	99	1	3	n1c(noc1c1ccncc1)c1ccc(NC(=O)c2c(F)cccc2)cc1	c1(c2ccccc2)noc(c3ccncc3)n1	2089 analogs, 117 refs	US20120263646
18	d	wact-190	9036812	98	3	6	n1c(noc1c1ccncc1)c1ccc(OCc2ccccc2)cc1			
19	d	wact-195	9040512	80	9	3	n1c(onc1c1ccc(OCc2ccccc2)cc1)c1ncccc1			
20	d	wact-713	7990228	51	5	2	n1c(noc1c1ccncc1)c1ccc(cc1)Cl			
21	e	wact-113	7834045	84	14	5	n1c(onc1c1ccc(cc1)Br)c1occc1	c1(c2ccco2)onc(c3ccccc3)n1	1493 analogs, 71 refs, 0 amy.ints	
22	e	wact-165	9020086	85	14	4	n1c(onc1c1ccc(cc1)F)c1occc1			
23	f	wact-58	6039582	62	34	4	n1c(noc1c1ccc(cc1)Cl)c1ncccc1	c1(c2ccccc2)onc(c3ccccn3)n1	2986 analogs, 183 refs, 0 amy.ints	
24	f	wact-153	9013537	59	38	5	n1c(noc1c1ccc(OCc2ccccc2)cc1)c1ncccc1			
25	f	wact-507	7629983	23	6	4	n1c(c2c(ccc(c2)Cl)Cl)onc1c1ncccc1			
26	g	wact-2	5185411	80	23	4	n1c(onc1c1ccc(cc1)Br)c1sccc1	c1(c2cccs2)onc(c3ccccc3)n1	4224 analogs, 429 refs, 0 amy.ints	
27	g	wact-136	7989399	48	31	4	n1c(onc1c1ccc(OC)ccc1)c1sccc1			
28	g	wact-169	9024879	69	35	4	n1c(noc1c1c(cc(cc1)Cl)Cl)c1sccc1			
29	g	wact-570	9028223	85	8	3	n1c(onc1c1ccc(NC(=O)c2c(F)cccc2)cc1)c1sccc1			
30	h	wact-391	5307255	100	0	3	[N+](=O)(c1ccc(N/C=C/C(=O)c2ccccc2)cc1)[O-]	O=C(c1ccccc1)/C=C/Nc2ccccc2	*1273 analogs, 110 refs	21755599, US9095596, US20120237446
31	h	wact-416	5404872	100	0	3	C(=C\Nc1ccc(Br)cc1)/C(=O)c1ccccc1			
32	h	wact-709-2	6088831	39	4	2	C(=C\Nc1c(F)cccc1)/C(=O)c1ccccc1			
33	h	wact-709-4	6642644	100	0	2	c1(cc(ccc1N/C=C/C(=O)c1ccccc1)Br)F			
34	h	wact-709-5	6669323	100	0	2	c1(cc(ccc1N/C=C/C(=O)c1ccccc1)F)Br			
35	h	wact-709-6	6872372	100	0	2	C(=C\Nc1ccc(Cl)cc1)/C(=O)c1ccccc1			
36	h	wact-709-8	7313533	99	2	2	c1(cc(N/C=C/C(=O)c2ccc(cc2)Br)ccc1F)F			
37	h	wact-709-9	6370432	100	0	2	C(=C\Nc1ccc(F)cc1)/C(=O)c1ccc(cc1)Br			
38	i	wact-49	5459938	88	15	3	N1(c2ccc(cc2)F)CCN(C2CCC(CC2)c2ccccc2)CC1	c1(N2CCN(CC2)C3CCCCC3)ccccc1	5265 analogs, 387 refs	DOI:10.1007/s11094-019-02000-
39	i	wact-50	5556756	99	2	8	[N+](=O)(c1ccc(N2CCN(C(=O)C(c3ccccc3)CC)CC2)cc1)[O-]	O=[N+]([O-])c1ccc(N2CCN(CC2)C(C)=O)cc1	9419 analogs, 407 refs	29394041, US20140187556
40	i	wact-364	5269853	69	22	3	[N+](=O)(c1ccc(N2CCN(C(=O)c3sccc3)CC2)cc1)[O-]	O=[N+]([O-])c1ccc(N2CCN(CC2)C(C)=O)cc1		
41	i	wact-381	5221072	100	1	4	[N+](=O)(c1ccc(N2CCN(C(=O)c3ccc(cc3)Br)CC2)cc1)[O-]	O=[N+]([O-])c1ccc(N2CCN(CC2)C(C)=O)cc1		
42	j	wact-51	5631017	51	28	4	Ic1cccc(c1)c1nnc(o1)c1ccccc1	c1(c2oc(c3ccccc3)nn2)ccccc1	*824 analogs, 118 refs	19651517, 23766818, 24936678, DOI: 10.1039/c3md00189j;
43	j	wact-425	5570574	47	16	5	Brc1ccc(cc1)c1nnc(o1)c1ccccc1			
44	k	wact-81	7634492	94	5	4	n1c(noc1/C=C/c1c(Cl)cccc1)c1ccncc1	c1(c2ccccc2)noc(/C=C/c3ccccc3)n1	6678 analogs, 16 refs	US8183276
45	k	wact-609	7750501	97	5	3	n1c(noc1/C=C/c1ccccc1)c1ccc(NC(=O)c2occc2)cc1			
46	l	wact-86	7640928	62	24	5	c1(oc2c(c1)cccc2)C(=O)Nc1cc(c(NC(=O)c2c(Cl)cccc2)cc1)O	O=C(c(c1)oc2c1cccc2)Nc3ccccc3	29324 structures, 811 refs, 0 amy.ints	
47	l	wact-134	7985302	46	40	6	c1(oc2c(c1)cccc2)C(=O)Nc1cc(c(N2CCN(C(=O)CC)CC2)cc1)Cl			
48	[redacted]	wact-15	7687977	86	38	7	n1c(sc2c1cccc2)COc1ccc(F)cc1	c1(COc2ccccc2)sc3ccccc3n1	3345 analogs, 258 refs, 0 amy.ints	
49	[redacted]	wact-24	5162985	70	13	4	n1c(cnc2c1cccc2)c1ccc(cc1)OCC	COc1ccc(c2cnc3ccccc3n2)cc1	9419 analogs, 407 refs	23047223, 33475377, US20020155172
50	[redacted]	wact-37	1	14	27	4	c1(=O)n(ncc(c1Cl)OC)c1cc(C(F)(F)F)ccc1	O=c1cc(OC)cnn1c2ccccc2	43522 analogs, 262 refs, 0 amy.ints	
51	[redacted]	wact-40	5360297	12	6	4	c1(nc2c(o1)cccc2)c1nc2c(cc1)cccc2	c1(c2ccc3ccccc3n2)oc4ccccc4n1	328 analogs, 25 refs, 0 amy.ints	
52	[redacted]	wact-102	7747740	45	31	5	O(c1ccc(cc1)OC)Cc1ccc(Cl)cc1	COc1ccc(OCc2ccccc2)cc1	*330 analogs, 474 refs	24936678, 26170205, WO2015090122
53	[redacted]	wact-105	7782912	99	2	5	c1(C(=O)O/N=C(/c2cccc2)\N)c(ccc(c1)Br)Cl	O=C(O/N=C(N)/c1ccncc1)c2ccccc2	79 analogs, 11 refs, 0 amy.ints	
54	[redacted]	wact-120	7889289	92	9	9	C(=O)(Nc1ccc(c2ccccc2)cc1)OC	C(=O)(Nc1ccc(c2ccccc2)cc1)OC	8518 analogs, 658 refs, 0 amy.ints	
55	[redacted]	wact-128	7971816	41	27	8	c1(C(=O)Nc2ccc(Br)cc2)c(cc(cc1)F)F	O=C(Nc1ccccc1)c2ccccc2	*10324 analogs, 127 refs	19191553, 21755599, 25515893, 26007606,
56	[redacted]	wact-220	5784085	99	2	4	Clc1ccc(cc1)N1CCN(CC1)/N=C\c1ccccn1	c1(N2CCN(/N=C\c3nccccc3)CC2)ccccc1	42 analogs, 8 refs, 0 amy.ints	
57	[redacted]	wact-390	5307019	88	2	3	n1c(noc1CCC)c1ccc(c2ccc(cc2)F)cc1	c1(c2ccc(c3ccccc3)cc2)nocn1	2994 analogs, 585 refs, 0 amy.ints	
58	[redacted]	wact-393	5308491	54	21	4	n1c(scc1c1ccc(cc1)I)Nc1ccc(Cl)cc1.Br	c1(Nc2ccccc2)scc(c3ccccc3)n1	19794 analgos, 828 refs, 0 amy.ints	
59	[redacted]	wact-415	5403320	100	0	4	c1(nc2c(s1)cccc2)c1ccc(NC(=O)c2c(F)cccc2)cc1	O=C(c1ccccc1)Nc2ccc(c3sc4ccccc4n3)cc1	1640 analogs, 83 refs	21755599,24297602, US20140105820
60	[redacted]	wact-446	5962739	80	28	3	c1(n[nH]c(c1)c1cc(F)ccc1)c1c(cc(cc1)C)O	c1(c2ccccc2)cc(c3ccccc3)[nH]n1	*5667 analogs, 2487 refs	US10435373
61	[redacted]	wact-469	6433196	98	4	6	n12c(nc3c1cccc3)SC(CC2=O)c1sccc1	n12c(nc3c1cccc3)SC(CC2=O)c1sccc1	2 analogs, 3 refs, 0 amy.ints	
62	[redacted]	wact-498	7426700	99	1	3	c1(c(=O)c2c(oc1)cc(cc2)OCC)c1ccc(cc1)Br	O=c1c2ccc(OCC)cc2occ1c3ccccc3	16848 analogs, 8384 refs	22587837, 23766818, 29191087, 32616652
63	[redacted]	wact-587	5175165	99	1	3	[N+](=O)(c1cc2c(nc1)cc(cc2)OC)[O-]	[N+](=O)(c1cc2c(nc1)cc(cc2)OC)[O-]	*101 analogs, 12 refs	30956012
64	[redacted]	wact-712-1	7972897	79	1	2	n1c(onc1c1ccc(cc1)Cl)c1ncccc1	c1(c2cccnc2)onc(c3ccccc3)n1	5088 analogs, 178 refs	US20110081297
65	[redacted]	dehydrovar	[redacted]	85	25	3	c12c(c3c(o1)cc(cc3)OC)COc1c2ccc(c1)OC	c12oc3ccccc3c1COc4ccccc42	70 analogs, 384 refs, 0 amy.ints	

Supplemental Table 3. A Literature-Based Search for Evidence of Amyloid Interaction Among 65 Crystalizing Molecules.

[a]The substructure that is in common to a group of molecules (aka the core scaffold) is depicted in Figure 2A.

[b]The Chembridge identification number for reordering at Chembridge Inc.

[c]The percentage of animals within the population, grown in 30 μM of compound, is shown, along with the standard of deviation (sd) and the number of independent biological repeats (N).

[d]The SMILES codes for the small molecule structure or the core scaffold used in SciFinder searches

[e]The number of analogs found in SciFinder searches using the core scaffold in substructure searches. The number of academic or patent-based publications (refs) associated with the analogs is also shown. In cases where searches with the core scaffold yielded >20,000 references, we instead used the primary structure to perform SciFinder searches and used a cutoff of 80% structural similarity or more to perform the searches. Searches performed this way are marked with an asterisks. The cell is colored pink if no evidence was found for amyloid interaction (0 amy.ints). The date of the searches is shown in brackets.

[f]The pubmed ID (PMID) and/or patent number is shown that provides evidence for a primary role in amyloid interaction. The date of the searches is shown in brackets.

Supplemental Table 4

	wactive	Chembridge ID[a]	Structure[b]	Common Substructure (aka Core Scaffold) [b]	SciFinder Scholar Substructure Search (2022-04) [c]	PMID/Patent (2022-04) [d]
1	wact-204	9063096	C1(CC1)NCc1ccc(OCc2ccc(Cl)cc2)cc1.Cl	C1(NCc2ccc(OCc3ccccc3)cc2)CC1	778 structtures- 54 refs- 0 amy.ints	
2	wact-35	5344384	n1(c2c(c3c1cccc3)cc(cc2)Cl)CO	c12ccccc1c3ccccc3n2	*595 analogs, 144 refs	34498871, WO2010092111, DOI:10.1021/acs.jpcb.1c06161
3	wact-614	9039813	c1(c2c(cc(cc2)Cl)Cl)oc(cc1)CNC1CC1.Cl	c1(c2ccccc2)ccc(CNC3CC3)o1	754 structtures- 26 refs- 0 amy.ints	
4	wact-1	5121613	c12nc(cn1ccs2)c1ccc(cc1)Cl	c12sccn1cc(c3ccccc3)n2	*358 analogs, 185 refs, 0 amy.ints	
5	wact-4	5352487	c1(oc(nn1)SCC)c1c(cc(cc1)Cl)Cl	CCSc1nnc(c2ccccc2)o1	*280 analogs, 65 refs, 0 amy.ints	
6	wact-7	5652963	o1nc(nc1c1cccs1)c1ccccc1	o1nc(nc1c1cccs1)c1ccccc1	4224 structures, 429 refs, 0 amy.ints	
7	wact-19	5104063	c12c(SCCc3ccncc3)cccc1cccc2	c12c(SCCc3ccncc3)cccc1cccc2	24 strctures, 2 papers, 0 amy.ints	
8	wact-139	9000613	n1c(onc1c1cc(Br)ccc1)c1occc1	c1(c2ccco2)onc(c3ccccc3)n1	1493 structures, 71 refs, 0 amy.ints	
9	wact-423	5547023	COc1ccc(CNc2ccc(Br)cc2)cc1	COc1ccc(CNc2ccccc2)cc1	*656 analogs, 51 refs, 0 amy.ints	
10	wact-596	5649594	Fc1ccccc1Nc1nc(cs1)c1ccccc1	c1(Nc2scc(c3ccccc3)n2)ccccc1	19794 structures, 828 refs, 0 amy.ints	
11	wact-23	5156707	c1(ncc(o1)c1ccc(cc1)C)c1ccncc1	c1(c2ccncc2)oc(c3ccccc3)cn1	550 structures, 240 refs, 0 amy.ints	
12	wact-29	5264250	s1c(ccc1CN1CCN(c2ccc(cc2)F)CC1)Br	c1(CN2CCN(CC2)c3ccccc3)sccc1	6636 analogs, 249 refs	WO2017159484; US8420640
13	wact-30	5267230	N1(c2ccc(cc2)F)CCN(Cc2cc(Br)ccc2)CC1	N1(CCN(CC1)Cc2ccccc2)c3ccccc3	*784 analogs, 34 refs, 0 amy.ints	
14	wact-481	6631407	n1c(scc1c1ccc(cc1)Cl)CC(=O)OCC	O=C(OCC)Cc1scc(c2ccccc2)n1	1246 structures, 43 refs, 0 amy.ints	
15	wact-521	7688376	c1(C(=O)NC(c2ccccc2)C)c(ccc(c1)Br)OCC	O=C(NCc1ccccc1)c2ccccc2	*2103 analogs, 79 refs, 0 amy.ints	
16	wact-54	5686969	n1c(noc1COc1ccc(Cl)cc1)c1cnccc1	c1(c2cccnc2)noc(COc3ccccc3)n1	186 structures, 25 refs, 0 amy.ints	
17	wact-560	9010683	C(=O)(Nc1c(Cl)cccc1)c1ccc(cc1)CC	O=C(c1ccccc1)Nc2ccccc2	*3616 analogs, 146 refs, 0 amy.ints	
18	wact-65	6858658	c1(C(=O)N2CCN(c3cc(C(F)(F)F)ccc3)CC2)c(ccc(c1)Cl)Cl	O=C(N1CCN(CC1)c2ccccc2)c3ccccc3	56127 structures, 1713 refs, 0 amy.ints	
19	wact-74	7597064	c1(ncccn1)SCc1ccc(Cl)cc1	c1(SCc2ccccc2)ncccn1	41555 structures, 928 refs, 0 amy.ints	
20	wact-11	6222549	C(c1c(C(=O)NCCc2ccc(Cl)cc2)cccc1)(F)(F)F	O=C(NCCc1ccccc1)c2ccccc2	*626 analogs, 53 refs, 0 amy.ints	
21	wact-103	7756678	C(=O)(c1sccc1)Nc1cc(c(N2CCN(CC2)CC)cc1)Cl	O=C(Nc1ccc(N2CCNCC2)cc1)c3sccs3	832 analogs, 39 refs, 0 amy.ints	
22	wact-121	7889470	c1(ncccn1)SCC#CCOc1ccc(Cl)cc1	c1(SCC#CCOc2ccccc2)ncccn1	*644 analogs, 15 refs, 0 amy.ints	
23	wact-132	7983837	S(=O)(=O)(c1ccc(c(cc1Cl)OCC)Cl)NCc1ccncc1	O=S(c1ccccc1)(NCc2ccncc2)=O	*15086 analogs, 428 refs, 0 amy.ints	
24	wact-141	9003606	C(=O)(Nc1ccc(Cl)cc1)Cc1cc(F)ccc1	O=C(Cc1ccccc1)Nc2ccccc2	*3663 analogs, 78 refs, 0 amy.ints	
25	wact-150	9012025	N1(c2c(cc(NC(=O)c3ccc(cc3)CC)cc2)Cl)CCN(CC1)C	O=C(c1ccccc1)Nc2ccc(N3CCNCC3)cc2	14917 analgos, 283 refs	US20110250135, 23008501 (the core is a small part of the molecule)
26	wact-160	9017218	C(=O)(C1CCN(CC1)CCOc1c(cc(cc1)Cl)C)OCC.Cl	O=C(OC)C1CCN(CCOc2ccccc2)CC1	2007 analogs, 99 refs, 0 amy.ints	
27	wact-161	9017369	n1c(nc(nc1Nc1ccc(Cl)cc1)N)C(F)(F)F	c1(Nc2ccccc2)ncncn1	*1117 analogs, 159 refs, 0 amy.ints	
28	wact-164	9020008	O(c1ccc(cc1)CNC)Cc1ccc(Cl)cc1.Cl	c1(OCc2ccccc2)ccccc1	*382 analogs, 16 refs	
29	wact-200	9053402	C(=O)(N1CCN(CC1)CCC)Nc1cc(cc(c1)Cl)Cl	O=C(Nc1ccccc1)N2CCNCC2	*1067 analogs, 22 refs, 0 amy.ints	
30	wact-380	5218876	C(=O)(c1sccc1)Nc1ccc(Cl)cc1	O=C(Nc1ccccc1)c2cccs2	*5859 analogs, 214 refs, 0 amy.ints	
31	wact-93	7695043	n1(c(nc2c1cccc2)c1scnc1)Cc1c(F)cccc1	n1(Cc2ccccc2)c3ccccc3nc1c4cncs4	32 analogs, 9 refs, 0 amy.ints	
32	wact-99	7747049	C(=O)(c1occc1)Nc1cc(c(N2CCN(CC2)CC)cc1)Cl	O=C(Nc1ccc(N2CCNCC2)cc1)c3ccco3	1386 analogs, 73 refs, 0 amy.ints	
33	wact-100	7747140	N(=C(\c1ccncc1)/N)/OC(=O)c1c(cc(cc1)C)C	O=C(c1ccccc1)O/N=C/c2ccncc2	320 analogs, 31 refs, 0 amy.ints	
34	wact-101	7747622	N1(C(=O)c2ccc(cc2)c2ccccc2)CC(CC1)c1ccccc1	N1(C(=O)c2ccc(cc2)c2ccccc2)CC(CC1)c1ccccc1	121 analogs, 8 refs, 0 amy.ints	
35	wact-104	7780917	C(=O)(O/N=C(/c1ccncc1)\N)C(Oc1ccc(Br)cc1)C	O=C(COc1ccccc1)O/N=C/c2ccncc2	99 analogs, 9 refs, 0 amy.ints	
36	wact-107	7785818	C(=S)(Nc1cc(c(cc1)Cl)Cl)NC1CCN(Cc2ccccc2)CC1	S=C(NC1CCN(CC1)Cc2ccccc2)Nc3ccccc3	505 analogs, 38 refs, 0 amy.ints	
37	wact-108	7788232	C(=S)(NC1CCN(Cc2ccccc2)CC1)NCc1ccc(Cl)cc1	S=C(NCc1ccccc1)NC2CCN(CC2)Cc3ccccc3	154 analogs, 6 refs, 0 amy.ints	
38	wact-109	7795345	[N+](=O)(c1ccc(NC(=S)NCc2cc(c(cc2)Cl)Cl)cc1)[O-]	O=[N+]([O-])c1ccc(NC(NCc2ccccc2)=S)cc1	1444 analogs, 108 refs, 0 amy.ints	
39	wact-111	7805914	C(=S)(N1CCN(c2cc(c(cc2)Cl)Cl)CC1)NCC1OCCC1	S=C(NCC1OCCC1)N2CCN(CC2)c3ccccc3	30 analogs, 0 refs, 0 amy.ints	
40	wact-112	7831354	C(c1cc(NC(=O)Nc2ccc(OC(F)F)cc2)ccc1)(F)(F)F	O=C(Nc1ccccc1)Nc2ccccc2	*250 analogs, 49 refs, 0 amy.ints	
41	wact-114	7837303	n1(ncc(c1)NC(=S)NCc1ccc(F)cc1)Cc1ccc(Br)cc1	S=C(NCc1ccccc1)Nc2cn(Cc3ccccc3)nc2	235 analogs, 0 refs, 0 amy.ints	
42	wact-115	7839427	[N+](=O)(c1ccc(N2CCN(C(=S)NCc3ccc(Cl)cc3)CC2)cc1)[O-]	O=[N+]([O-])c1ccc(N2CCN(CC2)C(NCc3ccccc3)=S)cc1	287 analogs, 5 refs, 0 amy.ints	
43	wact-117	7854576	[N+](=O)(c1cc(C(F)(F)F)ccc1NCCCNC(=O)c1ccc(cc1)F)[O-]	O=C(c1ccccc1)NCCCNc2ccccc2	132 analogs, 6 refs, 0 amy.ints	
44	wact-118	7862504	s1c(ccc1)CNCc1cc(OCc2ccccc2)ccc1.Cl	c1(CNCc2cccc(OCc3ccccc3)c2)cccs1	274 analogs, 16 refs, 0 amy.ints	
45	wact-12	7003409	c1(C(=O)NCCOc2ccc(cc2)CC)c(I)cccc1	O=C(NCCOc1ccccc1)c2ccccc2	*1582 analogs, 22 refs, 0 amy.ints	
46	wact-122	7930372	c1([N+](=O)[O-])c(cc(N2Cc3c(CC2)cccc3)c(c1)F)N1CCN(C(=O)C)CC1	c1(N2CCNCC2)cc(N3Cc4ccccc4CC3)ccc1	78 analogs, 10 refs	US20160283652, CA2735158
47	wact-125	7949759	c1(C(=O)NCCSC2CCCCC2)c(SC)cccc1	O=C(NCCSC1CCCCC1)c2ccccc2	1739 analogs, 27 refs, 0 amy.ints	
48	wact-127	7962412	CCCCCNC(=O)C1=CC=CC=C1SC	CCCCCNC(=O)C1=CC=CC=C1SC	23545 analogs, 409 refs, 0 amy.ints	
49	wact-13	7632721	n1c(noc1c1cc(ccc1)C)c1ccc(cc1)OC	c1(c2ccccc2)noc(c3ccccc3)n1	*2949 analogs, 121 refs	US20110081297, JP2009203166
50	wact-130	7974202	n1c(oc2c1cc(N)cc2)c1ccc(cc1)C(C)C	c1(c2ccccc2)oc3ccccc3n1	*1191 analogs, 168 refs, 0 amy.ints	
51	wact-137	7996054	n1c(oc2c1nccc2)c1cc(c(NC(=O)c2cc(Cl)ccc2)cc1)C	O=C(c1ccccc1)Nc2ccc(c3oc4cccnc4n3)cc2	449 structures, 19 refs, 0 amy.ints	
52	wact-143	9008780	c1(c(c(cc(c1)Cl)C)OCCCN1CCN(CC1)C)Br.Cl	c1(OCCCN2CCNCC2)ccccc1	*632 analogs, 4 refs, 0 amy.ints	
53	wact-144	9009342	c1(c(ccc(c1)I)OCCCN(C)C)C.Cl	CN(C)CCCOc1ccccc1	**75%, 1858 analogs, 31 refs, 0 amy.ints	
54	wact-146	9010643	N1(CCCCOc2ccc(c3ccccc3)cc2)CCOCC1.Cl	N1(CCOCC1)CCCCOc2ccc(c3ccccc3)cc2	33 structures, 33 refs, 0 amy.ints	
55	wact-147	9011168	c1(c2ccccc2)ccc(cc1)OCCNCC=C.Cl	C=CCNCCOc1ccc(c2ccccc2)cc1	18497 structures, 460 refs, 0 amy.ints	
56	wact-148	9011314	c1(c2c(ccc1OCCCn1cncc1)cccc2)Cl.Cl	c12ccccc1ccc(OCCCn3ccnc3)c2	557 structures, 28 refs, 0 amy.ints	
57	wact-151	9012797	N1(CCCOc2ccc(c3ccccc3)cc2)CCOCC1.Cl	N1(CCOCC1)CCCOc2ccc(c3ccccc3)cc2	247 structures, 83 refs, 0 amy.ints	
58	wact-155	9014681	C(c1cc(OCCCCn2cncc2)ccc1)(F)(F)(F)F.Cl	c1(OCCCCn2ccnc2)ccccc1	*28 analogs, 5 refs, 0 amy.ints	
59	wact-162	9018123	N(C(=O)c1occc1)(C(=O)c1occc1)c1ncc(cc1)I	O=C(c1ccco1)N(c2ccccn2)C(c3ccco3)=O	16 structures, 4 refs, 0 amy.ints	
60	wact-166	9023097	S(=O)(=O)(NCc1ccncc1)c1ccc(cc1)C1CCCCC1	S(=O)(=O)(NCc1ccncc1)c1ccc(cc1)C1CCCCC1	11 structures, 3 refs, 0 amy.ints	
61	wact-163	9018909	c12c(c(ccc1Cl)OCCNCC)cccc2.Cl	Clc1c2ccccc2c(OCCNCC)cc1	*262 structures, 23 refs, 0 amy.ints	
62	wact-365	5318059	C(=O)(c1cc(Cl)ccc1)N/N=C/c1ccc(SC)cc1	O=C(N/N=C/c1ccc(SC)cc1)c2ccccc2	*824 analogs, 118 refs	19651517, JP2009203166, DOI:10.1039/C3MD00189J

Supplemental Table 4. A Literature-Based Search for Evidence of Amyloid Interaction Among 62 Molecules that Fail to Form Crystals.

[a]The Chembridge identification number for reordering at Chembridge Inc.

[b]The SMILES codes for the small molecule structure or the core scaffold used in SciFinder searches.

[c]The number of analogs found in SciFinder searches using the core scaffold in substructure searches. The number of academic or patent-based publications (refs) associated with the analogs is also shown. In cases where searches with the core scaffold yielded >20,000 references, we instead used the primary structure to perform SciFinder searches and used a cutoff of 80% structural similarity or more to perform the searches. Searches performed this way are marked with an asterisks. The cell is colored pink if no evidence was found for amyloid interaction (0 amy.ints). The date of the searches is shown in brackets.

[e]The pubmed ID (PMID) and/or patent number is shown that provides evidence for a primary role in amyloid interaction. The date of the searches is shown in brackets.

Supplemental Table 5

Node ID[a]	cluster[b]	Name of Molecule	viability assay[c] DMSO n=2	w190 3.8 uM n=5	w11 10 uM n=3	Crystal Formation Assay[d] wact-190 + suppressor % crystals	n	SD	p value	Evidence for anti-amyloid activity (PubMed ID or Patent Number)[e]	Targeted Amyloid in Study	Aβ42 Secondary Fibril Inhibition Assay[f] Hit?	T-half mean	n	SD	p value
		solvent control										no	1.00	4	0	1
		solvent control	OG	0	0	100	4	0	na	none found	na	no	1.00	4	0	1
		positive control (Adapalene)										yes	4.12	4	1.2	1.2E-03
		positive control (Adapalene)										yes	4.17	4	2.3	1.8E-02
s1	a	RHAMNETIN	OG	OG	0	0	2	0	0.0E+00	16248550	Abeta42	no	0.93	4	0.1	6.5E-02
s2	a	BAICALEIN	OG	OG	0	42	3	25	1.6E-02	25043951, 23686791, 25043951, 25274114	Abeta42, IAPP					
s3	a	NOBILETIN	OG	OG	0	7	2	10	5.4E-03	none found	na					
s4	a	MORIN	OG	OG	0	27	4	40	1.0E-02	22762350, 16248550	Abeta42					
s5	a	FISETIN	OG	OG	0	29	2	11	1.2E-02	16248550, 18761054, 26944285	Abeta42	no	1.17	3	0.2	3.8E-02
s6	a	6,7-DIHYDROXYFLAVONE	OG	OG	0	0	2	0	0.0E+00	none found	na					
s7	a	KAEMPFEROL	OG	OG	0	4	2	5	1.5E-03	24468532, 16248550	Amylodosis, Abeta42, IAPP					
s8	a	HESPERETIN	OG	OG	0	20	4	15	4.0E-05	28672874, 22383310	Abeta42					
s9	a	SILIBININ	OG	OG	0	18	2	3	6.9E-04	21185897, 19552690	Abeta42					
s10	a	ISOGINKGETIN	OG	OG	0	3	2	4	8.6E-04	31697876	Abeta42					
s11	b	DICHLOROPHEN	sick	sick	0	19	4	26	7.6E-04	none found	na	yes	5.43	4	1.6	7.3E-04
s12	b	2,3,4-TRIHYDROXY-4'-ETHOXYBENZOPHENONE	OG	OG	0	14	3	12	2.3E-04	none found	na	no	0.86	3	0	1.7E-05
s13	b	3,4-DIDESMETHYL-5-DESHYDROXY-3'-ETHOXYSCLEROIN	OG	OG	0	20	4	13	1.7E-05	none found	na	no	0.90	3	0	4.2E-04
s14	b	CLOFOCTOL	OG	OG	0	0	2	0	0.0E+00	none found	na	yes	1.94	4	0.2	1.0E-05
s15	b	ROSOLIC ACID	OG	OG	0	70	2	1	1.6E-04	none found	na	no	1.32	3	0.1	3.2E-04
s16	c	PYROGALLIN	OG	OG	0	15	4	20	1.4E-04	US9463195B2	β-2 microglobulin fibril					
s17	c	PURPUROGALLIN-4-CARBOXYLIC ACID	OG	OG	0	74	2	0	1.6E-04	none found	na					
s18	c	METHYL 7-DESHYDROXYPYROGALLIN-4-CARBOXYLATE	OG	OG	0	0	2	0	0.0E+00	US9463195B2	β-2 microglobulin fibril					
s19	c	PURPUROGALLIN	OG	OG	0	0	2	0	0.0E+00	15611092, US9463195B2	Tau, β-2 microglobulin fibril	no	0.41	4	0.1	1.1E-04
s20	d	2,4-DINITROPHENOL	OG	OG	0	9	3	16	5.3E-04	16627944, 11344119, 11913969	TTR amyloid					
s21	d	OCTINOXATE	OG	OG	0	12	2	17	1.8E-02	none found	na	yes	1.66	4	0.5	1.5E-02
s22	d	DIIODOTYROSINE DIHYDRATE	OG	OG	0	11	2	7	2.7E-03	US20050038117A1	multiple					
s23	e	LAWSONE	OG	OG	0	22	2	7	4.4E-03	30704121	TTR amyloid	no	0.98	4	0.1	3.4E-01
s24	e	ANTHRACENE-1,4-DIONE	OG	OG	0	21	2	13	1.3E-02	none found	na					
s25	e	1,4-NAPHTHOQUINONE	OG	OG	0	0	2	0	0.0E+00	20709023, 31016960	Abeta42					
s26	f	ISOPOMIFERIN	OG	OG	0	2	3	3	6.1E-07	none found	na	no	1.25	4	0.2	1.1E-02
s27	f	ISOOSAJIN	OG	OG	0	21	2	13	1.2E-02	none found	na	no	1.42	3	0.1	2.9E-04
s28	f	MUNDULONE ACETATE	OG	OG	0	13	2	13	1.1E-02	none found	na	no	1.27	3	0.2	2.2E-02
s29	f	KOPARIN	OG	OG	0	12	2	11	7.5E-03	none found	na	no	1.00	3	0.1	4.4E-01
s30	g	PREGNENOLONE SUCCINATE	OG	OG	0	0	3	0	0.0E+00	none found	na	no	0.96	4	0.1	2.2E-01
s31	g	DESOGESTREL	OG	OG	0	17	2	8	4.4E-03	none found	na	yes	1.60	3	0.1	1.1E-04
s32	g	NORGESTIMATE	OG	OG	0	10	2	1	2.5E-05	none found	na	no	1.43	3	0.1	2.4E-04
s33	h	2',4'-DIHYDROXYCHALCONE	OG	OG	0	0	3	0	0.0E+00	none found	na	no	1.29	4	0.2	1.6E-02
s34	h	4'-HYDROXYCHALCONE	OG	OG	0	0	2	0	0.0E+00	none found	na	no	1.12	3	0	6.8E-09
s35	h	PHLORETIN	OG	OG	0	5	2	2	1.8E-04	none found	na	no	1.33	3	0.1	3.3E-04
s36	i	DIENESTROL	OG	OG	0	0	2	0	0.0E+00	none found	na					
s37	i	ONONETIN	OG	OG	0	0	3	0	0.0E+00	none found	na					
s38	i	DIETHYLSTILBESTROL	OG	OG	0	0	3	0	0.0E+00	15469931	amyloidosis	yes	2.41	4	0.6	1.5E-03
s39	j	CLIOQUINOL	OG	OG	0	9	2	13	9.9E-03	14676042, 21199452, 24591589	Abeta42					
s40	j	NITROXOLINE	OG	OG	0	53	4	35	3.7E-02	none found	na					
s41	k	MYCOPHENOLIC ACID	OG	OG	0	12	2	10	6.8E-03	none found	na	no	0.91	3	0	1.2E-04
s42	k	BENZYL BENZOATE	OG	OG	0	8	2	1	4.3E-05	none found	na	no	1.27	4	0.2	1.3E-02
s43	m	HAEMATOPORPHYRIN	OG	OG	0	0	2	0	0.0E+00	34570963	Abeta42	yes	2.17	4	0.7	9.4E-03
s44	m	PROTOPORPHYRIN IX	OG	OG	0	7	2	6	2.1E-03	34570963	Abeta42					
s45	m	CHLOROPHYLLIDE Cu COMPLEX Na	OG	OG	0	0	2	0	0.0E+00	none found	na					
s46	n	GOSSYPOL-ACETIC ACID COMPLEX	OG	OG	0	0	2	0	0.0E+00	none found	na					
s47	n	GOSSYPOL	OG	OG	0	0	3	0	0.0E+00	21858698, 25043951, 32210536	IAPP	yes	6.02	3	4.6	3.7E-02
s48		DEMECLOCYCLINE HYDROCHLORIDE	OG	sick	0	6	2	9	4.4E-03	21068391, 28338670	β-2 microglobulin fibril					
s49	r	DIHYDROCELASTROL	OG	OG	0	23	4	27	1.3E-03	none found	na	yes	1.90	4	0.1	1.2E-06
s50	r	CELASTROL	OG	OG	0	7	3	7	1.9E-05	none found	na	no	1.09	3	0.1	1.2E-02
s51	o	ALIZARIN	OG	OG	0	13	2	6	2.3E-03	34033711	insulin fibrils					
s52	o	PURPURIN	OG	OG	0	6	3	11	1.2E-04	34033711, 31562564	Insulin fibrils, Tau peptide					
s53	p	GLICLAZIDE	OG	OG	0	0	2	0	0.0E+00	none found	na	no	1.07	4	0.1	6.0E-02
s54	p	GLIMEPIRIDE	OG	OG	0	4	3	2	1.9E-07	none found	na	no	0.95	3	0	4.4E-02
s55	p	GLIPIZIDE	OG	OG	0	28	2	9	8.3E-03	none found	na	no	1.04	3	0	1.8E-02
s56	q	RAFOXANIDE	OG	OG	0	8	2	12	8.2E-03	none found	na	yes	23.16	3	4.1	5.2E-05
s57	q	CLOSANTEL	sick	sick	0	0	3	0	0.0E+00	none found	na	yes	28.00	3	6.7	2.0E-04
s58	q	OXYCLOZANIDE	OG	OG	0	27	4	30	2.6E-03	none found	na	no	1.42	3	0.1	9.8E-04
s59		LEOIDIN	OG	OG	0	8	2	4	7.3E-04	US9463195B2	β-2 microglobulin					
s60		TENIPOSIDE	OG	OG	0	27	2	0	1.7E-05	none found	na	no	0.93	3	0	7.2E-03
s61		DIFFRACTAIC ACID	OG	OG	0	46	2	6	5.9E-03	none found	na	no	1.16	3	0.1	2.0E-02
s62		BROMOCRIPTINE MESYLATE	OG	OG	0	0	2	0	0.0E+00	none found	na	no	0.74	3	0.1	7.9E-05
s63		ADAPALENE	OG	OG	0	10	2	10	5.7E-03	28011763	Abeta42					
s64		ERYTHROSINE SODIUM	OG	OG	0	4	3	3	1.1E-06	21354256, 28137461	lysozyme fibrils					
s65		ITRACONAZOLE HYDROCHLORIDE	OG	sick	0	25	2	8	5.2E-03	none found	na	no	0.78	3	0.1	5.4E-03
s66		NIFUROXAZIDE	OG	OG	0	24	4	32	3.1E-03	none found	na	no	0.97	3	0.1	2.4E-01
s67		NITAZOXANIDE	OG	OG	0	3	3	6	8.4E-06	none found	na	no	0.96	3	0.1	1.3E-01
s68		HARMALINE	OG	OG	0	36	2	1	4.4E-05	none found	na	unc	na	3	na	na
s69		alpha-MANGOSTIN	OG	OG	0	0	3	0	0.0E+00	21958557; 28429536; 32419519	Abeta42; amyloidosis					
s70		THIOSTREPTON	OG	OG	0	8	2	11	7.1E-03	none found	na	no	0.76	3	0.3	1.0E-01
s71		APOMORPHINE HYDROCHLORIDE	OG	sick	0	25	2	1	1.3E-04	none found	na	unc	na	3	na	na
s72		USNIC ACID	OG	OG	0	4	2	6	1.9E-03	none found	na	no	1.30	4	0.2	1.4E-02
s73		BITHIONATE SODIUM	sick	sick	0	0	2	0	0.0E+00	none found	na	unc	na	3	na	na
s74		CITRININ	OG	OG	0	13	4	26	4.9E-04	none found	na	yes	1.56	3	0.6	4.7E-02
s75		EBSELEN	OG	OG	0	21	2	6	3.3E-03	none found	na	no	1.03	3	0	1.4E-01
s76		CANDESARTAN CILEXTIL	OG	OG	0	0	2	0	0.0E+00	none found	na	yes	3.00	3	0.8	1.7E-03
s77		TOTAROL	OG	OG	0	0	2	0	0.0E+00	none found	na	yes	1.72	3	0.1	1.6E-06
s78		CURCUMIN	OG	OG	0	3	3	4	2.9E-06	15590663, 17472706, 18189141	Abeta42	no	0.39	4	0.3	1.8E-03
s79		4,4'-DIMETHOXYDALBERGIONE	OG	OG	0	0	2	0	0.0E+00	none found	na	no	1.24	3	0.2	1.6E-02
s80		DIHYDROGAMBOGIC ACID	OG	OG	0	12	2	8	4.0E-03	none found	na	no	0.78	3	0.1	1.5E-04
s81		ISORESERPINE	OG	OG	0	6	2	1	9.0E-05	none found	na	no	0.62	3	0.1	8.1E-05
s82		SAFROLE	OG	OG	0	12	2	16	1.7E-02	none found	na	no	0.92	3	0.1	1.1E-02
s83		TRICLABENDAZOLE	OG	OG	0	20	4	28	1.3E-03	34547896	TTR amyloid					
s84		ARIPIPRAZOLE	OG	sick	0	6	2	8	3.4E-03	none found	na	yes	2.26	3	1.2	4.2E-02
s85		SIROLIMUS	OG	OG	0	11	2	16	1.6E-02	none found	na	no	0.46	3	0	4.9E-07

Supplemental Table 5. 85 Spectrum Suppressors of Small Molecule Crystallization in the Pharynx Cuticle.

[a]The node ID is the label of the node shown in Figure 4a.

[b]The cluster letter is that given to scaffold clusters shown in Figure 4a and 4b.

[c]The viability assay is the standard six day viability assay described in the methods. The number of replicates (n) is shown, and the mode is shown. OG, a culture overgrown with worms; sick, a culture with 11-50 worms; 0, a culture with 0-10 worms.

[d]The crystal formation assay is described in the methods section.

[e]The pubmed ID or patent number is shown that provides evidence for a primary role in fibril inhibition.

[f]Hits equate to those molecules that significantly ($p<0.05$) antagonize Aβ42 secondary fibril formation by more than 50% that of the solvent control as measured by the time of half (T-half) saturated signal (see methods).

	Trivial Name	MolPort ID	Analog Smiles	Suppressor Analog[a]	48 hour crystal assay[b]			
					mean	n	sem	type
1	DMSO	negative control	na	na	0	6	0	-
2	wact-190	positive control	na	na	100	6	0	cry
3	RS-15	MolPort-001-814-824	c1cc2c(oc3ccc(cc3c2=O)Br)cc1	alpha-MANGOSTIN	100	4	0	cry
4	RS-50	MolPort-003-712-626	O=C1c2cc(ccc2C(=O)c2c1cccc2)F	PURPURIN/ALIZARIN	87	4	3	cry
5	RS-9	MolPort-002-211-224	O=C(c1ccc(OCC)cc1)c1ccc(cc1Cl)Cl	DDE	67	5	9	sph
6	RS-14	MolPort-000-690-079	c1(cc2c(oc3ccc(cc3c2=O)F)cc1)F	alpha-MANGOSTIN	66	4	12	cry
7	RS-11	MolPort-008-682-078	O=C(c1ccc(OCC)cc1)c1ccccc1Cl	DDE	60	3	19	sph
8	RS-40	MolPort-000-628-186	O=C1c2c(cccc2C(=O)c2c1cccc2)Cl	PURPURIN/ALIZARIN	56	5	7	cry
9	RS-6	MolPort-002-120-487	O=C(c1ccc(OC)cc1)c1ccc(cc1Cl)Cl	DDE	51	5	10	sph
10	RS-13	MolPort-001-814-873	O=C(c1ccc(cc1)F)C=Cc1c(cccc1)Cl	4'-HYDROXYCHALCONE	45	3	11	sph
11	RS-7	MolPort-002-120-597	O=C(c1ccc(OC)cc1)c1ccccc1Cl	DDE	41	3	10	sph
12	RS-41	MolPort-000-628-197	O=C1c2cccc(c2C(=O)c2c1cccc2Cl)Cl	PURPURIN/ALIZARIN	35	5	3	cry
13	RS-8	MolPort-002-209-464	O=C(c1ccc(OCC)cc1)c1ccc(cc1)Cl	DDE	26	5	6	cry
14	RS-10	MolPort-003-801-426	O=C(c1ccc(OC)c(c1)Cl)c1ccccc1	DDE	22	5	8	sph
15	RS-1	MolPort-000-153-180	O=C(c1ccc(OC)cc1)c1cccc(c1)Cl	DDE	14	5	7	sph
16	RS-46	MolPort-002-139-631	O=C1c2c(cccc2C(=O)c2c1cccc2)Br	PURPURIN/ALIZARIN	6	2	6	cry
17	RS-2	MolPort-000-153-182	O=C(c1ccc(OC)cc1)c1ccc(cc1)Cl	DDE	0	5	0	-
18	RS-5	MolPort-001-773-641	O=C(c1ccc(OC)cc1)c1ccc(cc1)F	DDE	0	4	0	-
19	RS-12	MolPort-009-323-013	O=C(c1ccc(OC)cc1Cl)c1ccccc1	DDE	0	5	0	-
20	RS-16	MolPort-000-153-368	O=C(Cc1ccccc1)c1ccc(cc1)Cl	ONONETIN	0	4	0	-
21	RS-18	MolPort-001-785-660	O=C(Cc1ccc(cc1)Cl)c1ccccc1	ONONETIN	0	4	0	-
22	RS-21	MolPort-002-498-703	O=C(Cc1ccc(c(c1)F)F)c1ccccc1	ONONETIN	0	4	0	-
23	RS-24	MolPort-003-899-970	O=C(Cc1ccc(cc1)F)c1ccc(cc1)Cl	ONONETIN	0	2	0	-
24	RS-26	MolPort-011-192-811	O=C(Cc1ccc(cc1)F)c1ccc(cc1Cl)Cl	ONONETIN	0	2	0	-
25	RS-27	MolPort-011-790-797	O=C(Cc1ccc(cc1Cl)Cl)c1ccc(cc1)Cl	ONONETIN	0	2	0	-
26	RS-28	MolPort-011-912-385	O=C(Cc1ccc(cc1)Cl)c1cccc(c1)F	ONONETIN	0	4	0	-
27	RS-29	MolPort-011-912-395	O=C(Cc1cccc(c1)F)c1cccc(c1)F	ONONETIN	0	4	0	-
28	RS-30	MolPort-011-912-620	O=C(Cc1ccc(cc1Cl)Cl)c1ccc(cc1)F	ONONETIN	0	4	0	-
29	RS-31	MolPort-012-334-336	O=C(Cc1ccc(cc1)Cl)c1ccc(cc1Cl)Cl	ONONETIN	0	2	0	-
30	RS-32	MolPort-013-275-146	O=C(Cc1cccc(c1)F)c1ccc(cc1)F	ONONETIN	0	4	0	-
31	RS-33	MolPort-013-289-535	O=C(Cc1cccc(c1)F)c1ccc(c(c1)Cl)Cl	ONONETIN	0	4	0	-
32	RS-38	MolPort-026-446-172	O=C(Cc1ccc(c(c1)F)F)c1ccc(cc1)Cl	ONONETIN	0	2	0	-
33	RS-45	MolPort-002-136-236	O=C1c2c(c(c(c(c2C(=O)c2c1cccc2)F)F)F)F	PURPURIN/ALIZARIN	0	2	0	-
34	RS-47	MolPort-002-250-630	O=C1c2c(c(c(c(c2C(=O)c2c1cccc2)Cl)Cl)Cl)Cl	PURPURIN/ALIZARIN	0	4	0	-
35	RS-48	MolPort-002-904-427	O=C1c2c(ccc(c2C(=O)c2c1cccc2)F)F	PURPURIN/ALIZARIN	0	4	0	-

Supplemental Table 6. Reduced Analogs of Suppressors.

Suppressors are listed in order of their ability to induced object formation.

[a]DDE, 3,4-DIDESMETHYL-5-DESHYDROXY-3'-ETHOXYSCLEROIN

[b]N, the number of trials (at least 20 animals were counted in each trial); SEM, standard error of the mean; type (of object) is either birefringent crystals (cry) or non-birefringent globular spheres (sph).

	Trivial Name	MolPort ID	Analog Smiles	Wactive Analog	6 day viability assay[a]						crystal counts[b]	Aβ42 Secondary Fibril Inhibition Assay[c]				
					DMSO	DMSO	DMSO	w190	w190	w190	w190					
					trial 1 (n=3)	trial 2 (n=3)	trial 3 (n=3)	trial 1 (n=3)	trial 2 (n=3)	trial 3 (n=3)	average +/- SEM (N=5, n>20)	Hit?	T-half mean	n	SD	p value
1		DMSO (n=6)			OG	OG	OG	let	let	let	100 +/- 0	no	1.00	4	0	1
2	OC-1	MolPort-000-132-940	c1cc(c2nc(c3cccnc3)no2)c(cc1)O	wact-10-2	OG	OG	OG	let	let	let						
3	OC-2	MolPort-001-849-559	c1cccc(OCc2nc3ccccc3s2)c1O	wact-15	let	OG	OG	let	let	let						
4	OC-4	MolPort-000-369-009	c1ccccc1c1nnc(c2c(cccc2)O)o1	wact-51	OG	OG	OG	let	let	let						
5	OC-5	MolPort-000-156-303	O=C(c1ccccc1)Nc1cccc(c1)O	wact-128	OG	OG	OG	let	let	let						
6	OC-6	MolPort-000-516-315	O=C(c1ccccc1)Nc1ccc(cc1)O	wact-128	OG	OG	OG	let	let	let						
7	OC-7	MolPort-000-677-289	O=C(c1ccc(cc1)O)Nc1ccccc1	wact-128	OG	OG	OG	let	let	let						
8	OC-8	MolPort-001-011-775	O=C(c1ccccc1)Nc1ccccc1O	wact-128	OG	OG	OG	let	let	let						
9	OC-9	MolPort-001-781-621	O=C(c1c(cccc1)O)Nc1ccccc1	wact-128	OG	OG	OG	let	let	let						
10	OC-10	MolPort-001-783-472	O=C(c1c(cccc1)O)Nc1ccc(cc1)O	wact-128	OG	OG	OG	let	let	let						
11	OC-11	MolPort-002-323-598	O=C(c1ccc(cc1)O)Nc1ccc(cc1)O	wact-128	OG	OG	OG	OG	OG	OG	57 +/- 16 (p <0.3)	no	1.15	4	0.13	2.9E-02
12	OC-12	MolPort-003-855-287	O=C(c1cc(ccc1)O)Nc1ccccc1	wact-128	OG	OG	OG	let	let	let						
13	OC-13	MolPort-046-069-921	O=C(c1ccccc1)Nc1ccc(cc1O)O	wact-128	OG	OG	OG	let	let	let						
14	OC-14	MolPort-008-388-876	c1cccc(c1c1nc(c2cccs2)no1)O	wact-169	OG	OG	OG	let	let	let						
15	OC-16	MolPort-001-900-048	c1cccc(c1c1nc(c2ccccc2)no1)O	wact-184	sick	OG	OG	let	let	let						
16	OC-17	MolPort-002-222-727	Brc1ccc(cc1)c1noc(c2ccc(cc2)O)n1	wact-184	OG	OG	OG	sick	OG	OG	0 +/- 0 (p =0)	yes	11.71	4	3.01	1.9E-04
17	OC-18	MolPort-000-519-488	c1ccccc1c1csc(Nc2cc(ccc2)O)n1	wact-393	sick	OG	OG	sted/dea	sick	let						
18	OC-20	MolPort-001-998-500	c1cc(c(cc1c1csc(Nc2ccccc2)n1)O)O	wact-393	OG	OG	OG	OG	OG	OG	46 +/- 17 (p <0.02)	no	1.40	4	0.17	1.5E-03
19	OC-21	MolPort-001-998-519	c1cc(cc(c1c1csc(Nc2ccc(cc2)O)n1)O)O	wact-393	OG	OG	OG	sick	OG	OG	24 +/- 7 (p <0.001)	no	1.46	4	0.30	1.1E-02
20	OC-22	MolPort-002-013-480	c1cc(ccc1c1csc(Nc2ccc(cc2)O)n1)O	wact-393	OG	OG	OG	sick	OG	OG	23 +/- 7 (p <0.001)	no	1.37	4	0.32	3.0E-02
21	OC-23	MolPort-002-176-399	Br.Oc1ccc(Nc2nc(cs2)-c2ccccc2)cc1	wact-393	OG	OG	OG	let	let	let						
22	OC-24	MolPort-002-973-587	c1cccc(c1c1csc(Nc2ccccc2)n1)O	wact-393	OG	OG	OG	let	let	let						
23	OC-25	MolPort-001-945-190	O=C(Nc1ccc(c(c1)O)c1nc2ccccc2s1)c1ccccc1	wact-415	OG	OG	OG	let	let	sick						
24	OC-26	MolPort-001-945-191	O=C(c1c(cccc1)F)Nc1ccc(c(c1)O)c1nc2c(cccc2)s1	wact-415	sick	OG	OG	let	let	let						
25	OC-27	MolPort-003-180-443	c1ccccc1c1nnc(c2ccc(cc2)O)o1	wact-425	OG	OG	OG	let	let	let						
26	OC-29	MolPort-010-675-363	Clc1ccc(cc1)c1noc(c2c(nccc2)O)n1	wact-712-1	OG	OG	OG	let	let	let						

Supplemental Table 7. Hydroxylated Analogs of Crystal-Forming Molecules.

[a]OG, the majority of the wells in the trial were over-grown with more than 50 animals in each well; sick, the majority of the wells in the trial were sick with between 11 and 50 animals in each well; let, the majority of the wells in the trial had 10 or fewer animals.

[b]N is the number of trials; n is the number of animals counted in each trial; SEM is the standard error of the mean; the p value shown is from a Student's T-test between the experimental sample and the wact-190-only control.

[c]Hits equate to those molecules that significantly (p<0.05) antagonize Aβ42 secondary fibril formation by more than 50% that of the solvent control as measured by the time of half (T-half) saturated signal (see methods).

Supplemental Figure 1. Crystallizing Small Molecules Grouped According to Structural Similarity. Small molecules belonging to structurally distinct families are boxed together. The 18 singletons are unboxed. The cluster that each boxed set of molecules belong to corresponds to the notation in Figure 3 and is indicated in the upper left-hand corner. Wactive names highlighted in pink have core scaffolds that are known to interact with amyloids (see methods and Supplemental Data File 1 for details). Molecule names that are underlined were discovered from a screen of the RLL1200 small molecule library.

Supplemental Figure 2. Further Details on the Biophysical Characterization of wact-190 and wact-416 *in vitro* Crystals. A-C. Different aspects of the 3D packing arrangement of wact-190 crystals from the a, b, and c aspects, respectively. **D.** The fitting pattern of wact-190 was obtained from the PXRD instrument. **E-G.** Different aspects of the 3D packing arrangement of wact-416 crystals from the a, b, and c aspects, respectively. **D.** The fitting pattern of wact-416 was obtained from the PXRD instrument. Panels (D) and (H) show the experimental powder diffraction profile (°), the calculate curve by using the reported structure (green line), the peak positions (|), and the normalized difference curve (I_o-I_c) (black curve).

Supplemental Figure 3. Crystal-Induced Disruption of the ABU-14::sfGFP Pharyngeal Cuticle Marker. A-C. Images of animals expressing ABU-14::sfGFP (the extrachromosomal array, which we integrated as *trIs113*, was a kind gift from David

23 Raizen) and stained with the indicated dyes. The imaging channel is indicated (lower
24 left) as is the 3-hour wactive treatment (left-hand side of micrograph series). DIC,
25 differential interference contrast; bire, birefringence; CFW, calcofluor white. Merge 1 is
26 the merge of ABU-14::GFP and the CFW signal. Merge 2 is the merge of the signals from
27 ABU-14::GFP and the birefringence signal. Blue arrows indicate overlapping signals of
28 the amyloid-binding dye and birefringence; orange arrows show a lack of amyloid-
29 binding dye signal associated with birefringence signal. 60 μM of wact-190 and wact-390
30 was used in all experiments relevant to panels A-C.
31
32 **Supplemental Figure 4. Larger wact-190 Crystals Often Fail to Overlap with Cuticle**
33 **Markers.** Legend is the same as that described for Figure 4 and Supplemental Figure 3.
34
35 **Supplemental Figure 5. Fluorescent Suppressors Specifically Localize to the Pharyngeal**
36 **Cuticle. A.** Calcofluor white (CFW) is used as counter-stain control for each of the
37 molecules (60 μM) examined. **B-C.** B. Whole animal pictures illustrating the specificity of
38 the localization of the indicated suppressor molecules. The intestine exhibits
39 autofluorescence from gut granules, as illustrated in the no-dye control pictures (C). ac,
40 anterior corpus; i, intestine.
41
42 **Supplemental Figure 6. The Construction and Analysis of a Random Network from the**
43 **Spectrum Library. A.** A structural similarity network of the 100 randomly chosen
44 Spectrum library molecules. The nodes (circles) represent a drug or natural product

45 whose number corresponds to the identity indicated in panel B. The links (straight lines)
46 represent a Tanimoto score of structural similarity of 0.8 or more (see methods). A bold
47 red outline indicates that the molecule is a known disruptors of amyloid fibril formation
48 (see panel B for details). **B.** The 100 molecules randomly chosen from the Spectrum
49 Library that were used the build the network depicted in panel A. The node ID is the
50 label of the node shown in panel A. The PubMed ID is shown for those molecules for
51 which evidence could be found of a primary role in fibril inhibition.
52
53 **Supplemental Figure 7. A-E. Behaviour of 2 mM Aβ42 Incubated with Small Molecules**
54 **under Different Aggregation Conditions. A.** Dichlorophen **B.** Candesartan Cilexetil **C.**
55 Closantel **D.** Gossypol **E.** OC-11, OC-17, OC-20, OC-21, OC-22 in **i.** unseeded conditions or
56 with **ii.** 1 mM monomer equivalent pre-formed seed (heavy seeded). Heavy seeded
57 conditions isolate elongation as the dominant mechanism of aggregation, as the
58 availability of fibril ends is so high that further amyloid formation only occurs via this
59 route. By comparison, light seeded conditions (main text) are dominated by secondary
60 nucleation and elongation, while under unseeded conditions primary nucleation,
61 secondary nucleation and elongation are operative.
62

Supplemental Figure 1

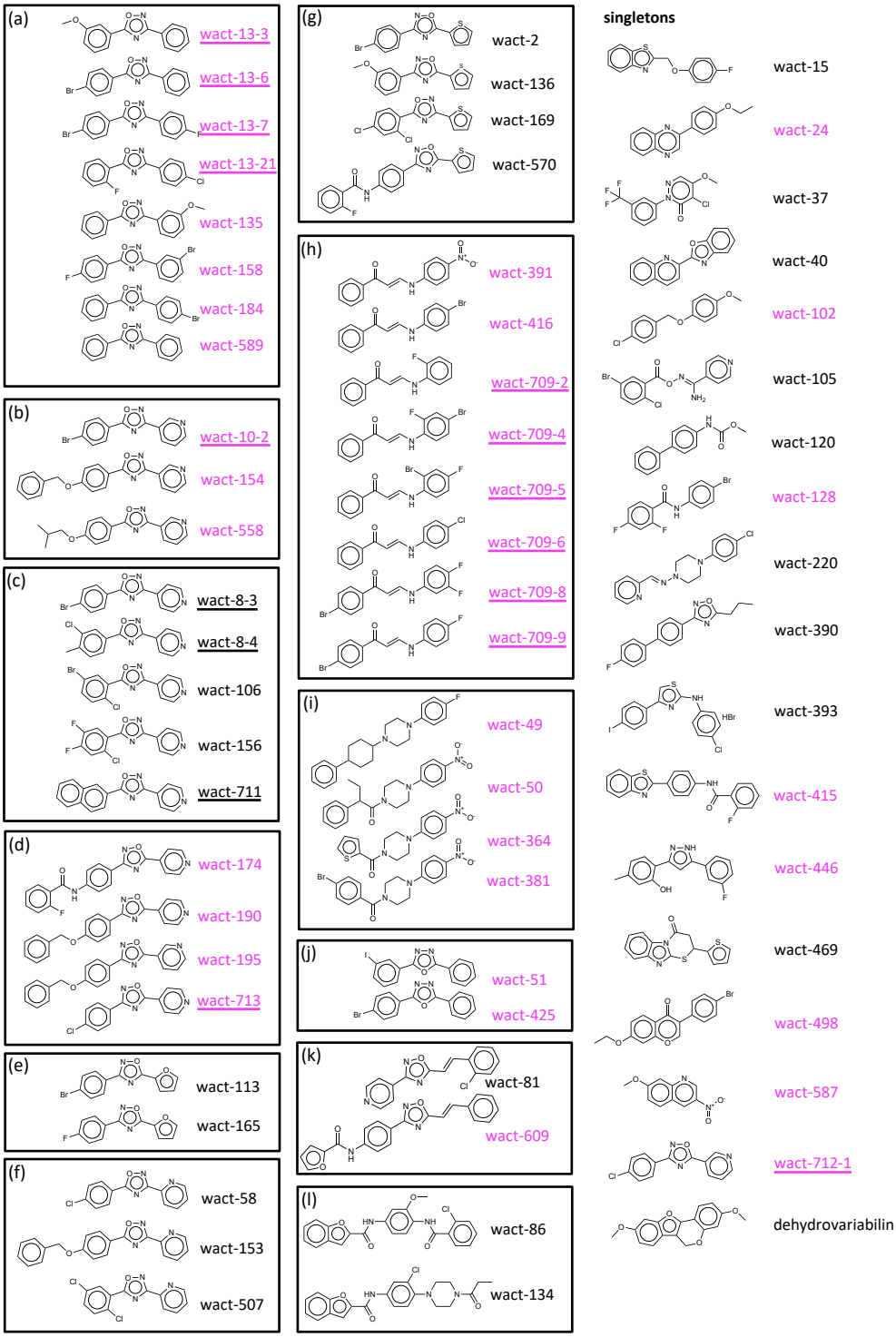

pink indicates the scaffold has been showin to interact with amyloids

Supplemental Figure 2

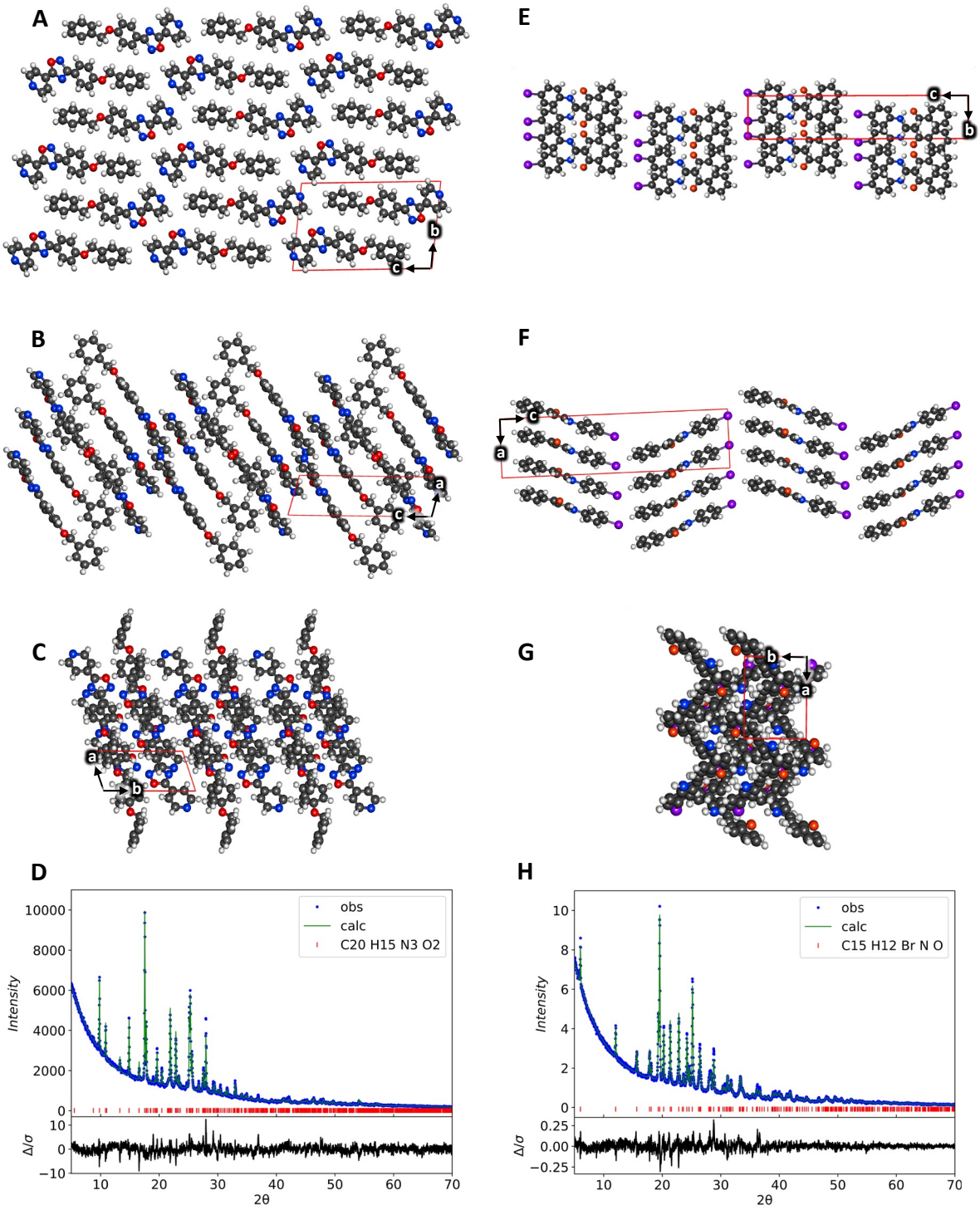

Supplemental Figure 3

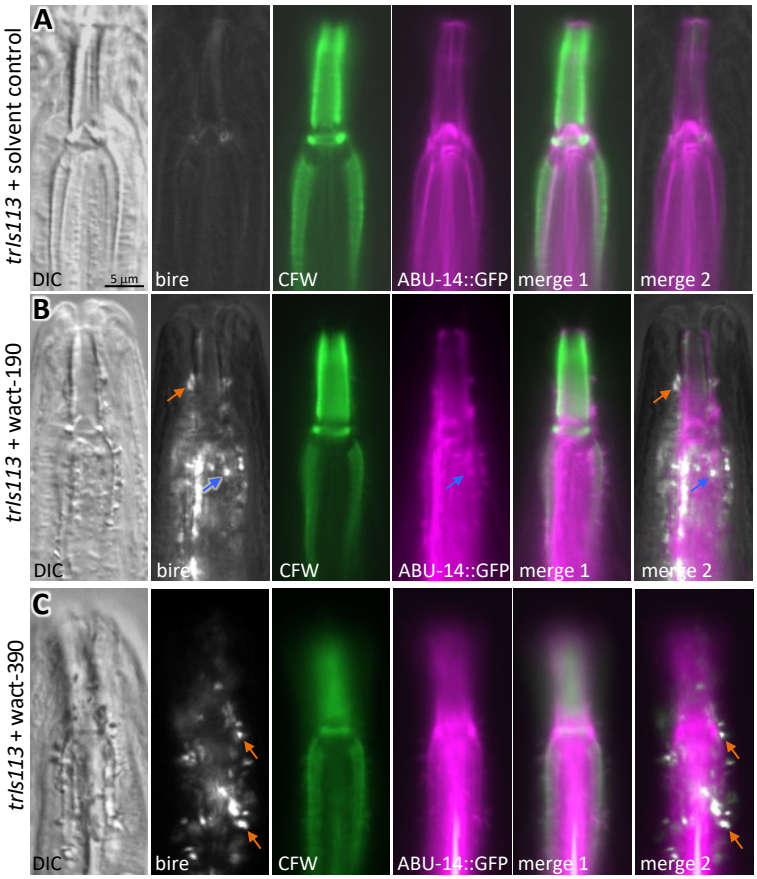

Supplemental Figure 4

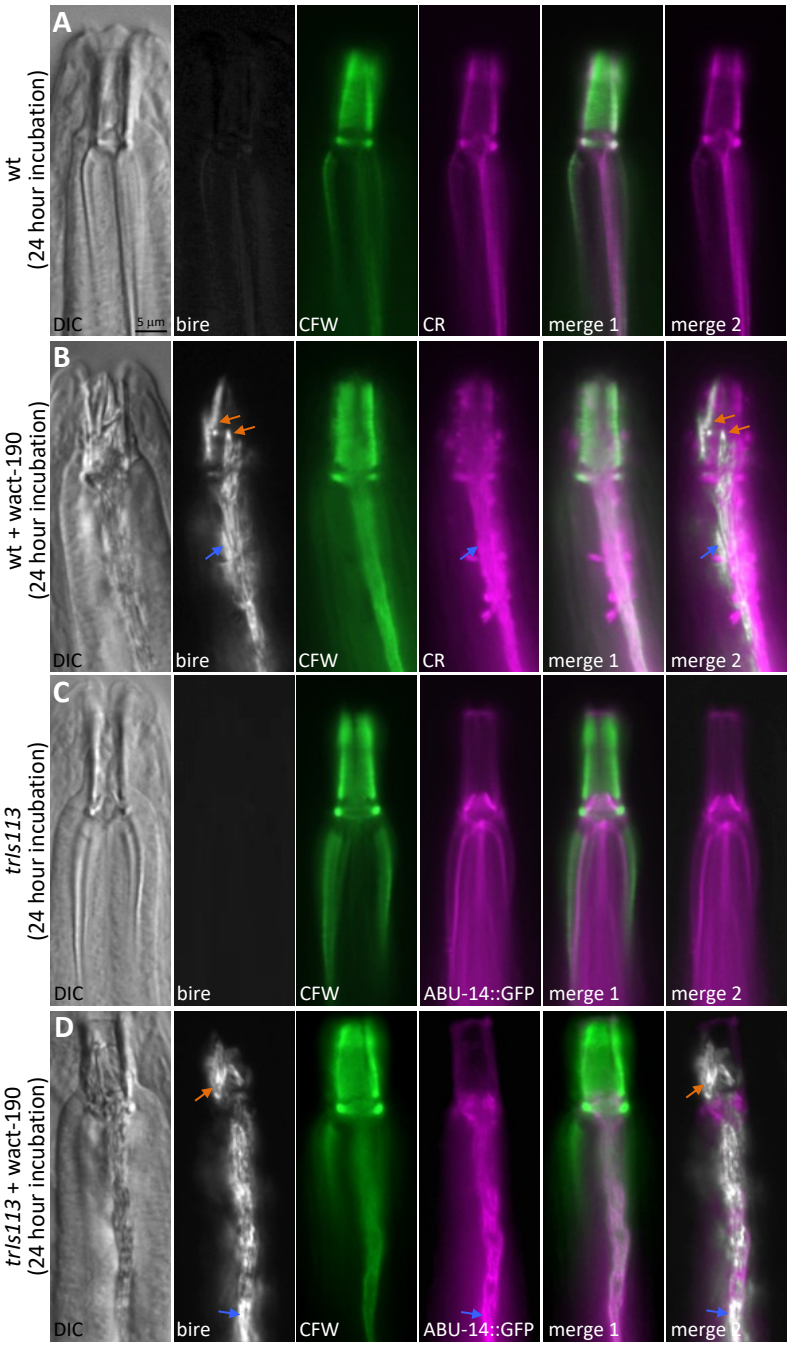

Supplemental Figure 5

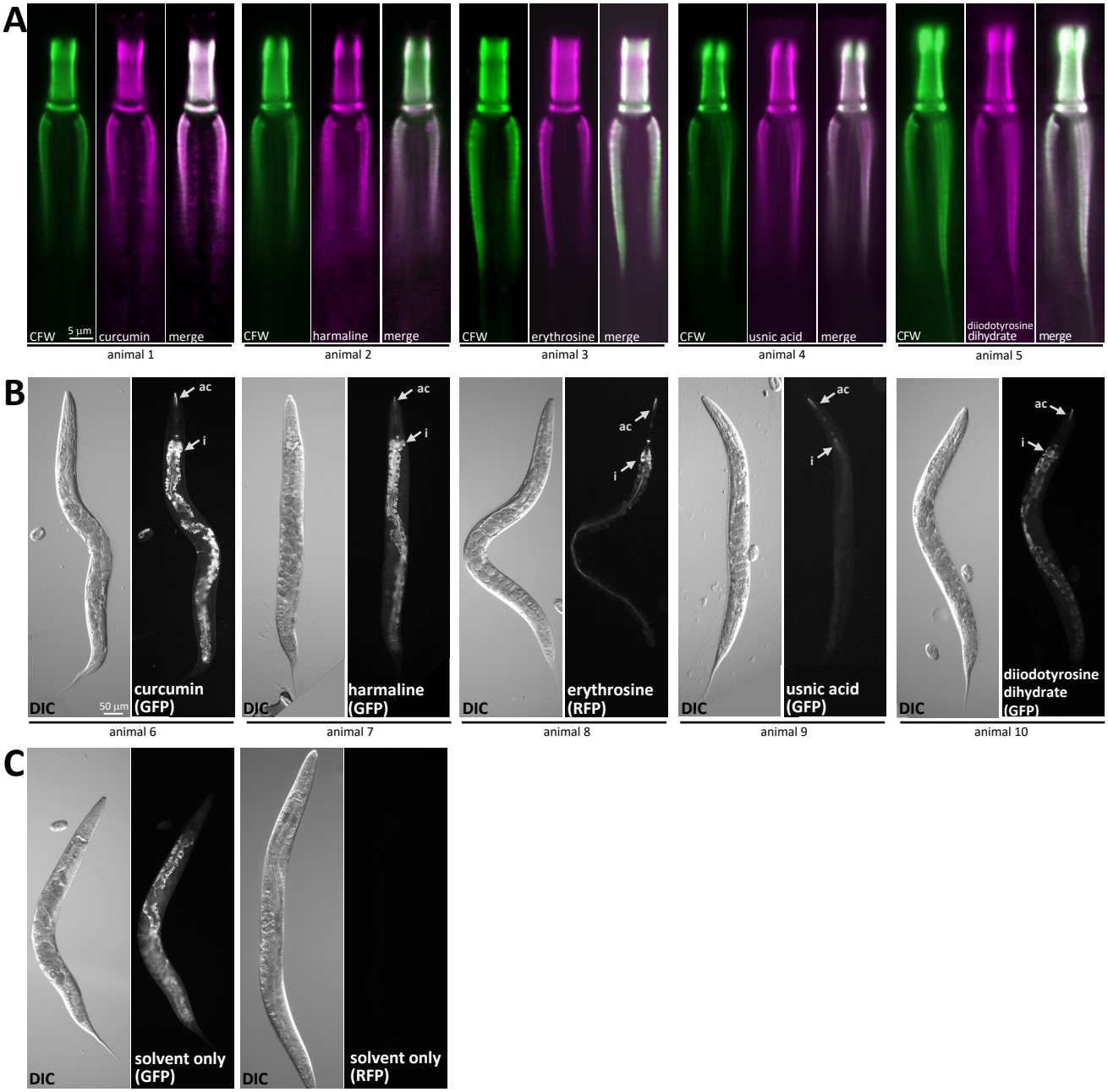

Supplemental Figure 6

A

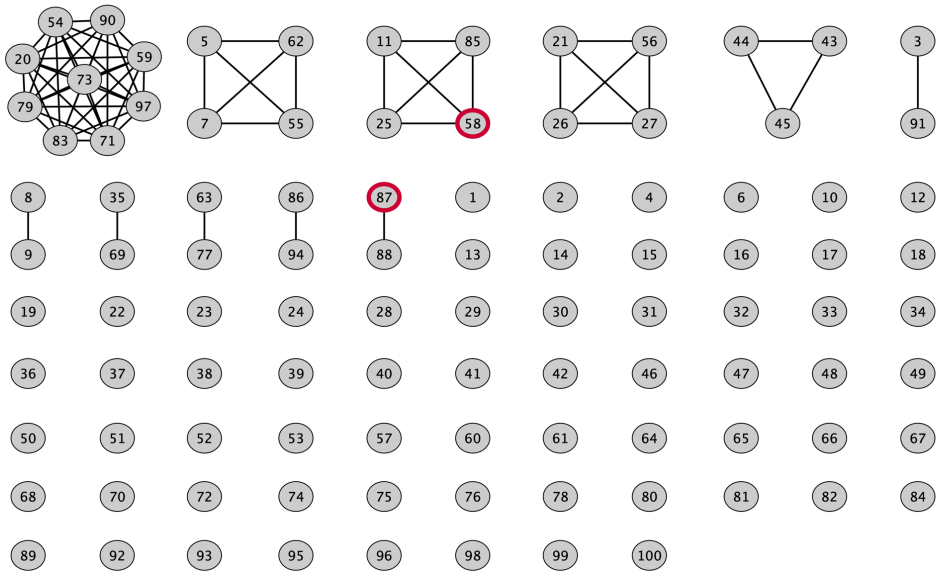

B

Node ID	Name of Molecule	Evidence for direct disruption of amyloid fibrils (PMID)	Targeted Amyloid
1	1,3-DIDEACETYL-7-DEACETOXY-7-OXOKHIVORIN	none	na
2	3-ACETAMIDOCOUMARIN	none	na
3	4,6-DIMETHOXYTOLUQUINONE	none	na
4	5-AMINOPENTANOIC ACID HYDROCHLORIDE	none	na
5	6,4'-DIMETHOXYFLAVONE	none	na
6	7-METHOXYCHROMONE	none	na
7	7,8-DIMETHOXYFLAVONE	none	na
8	8-HYDROXYCARAPINIC ACID	none	na
9	8beta-HYDROXYCARAPIN, 3,8-HEMIACETAL	none	na
10	ACETOHEXAMIDE	none	na
11	ACTINOQUINOL SODIUM	none	na
12	AMLEXANOX	none	na
13	ANAZOLENE SODIUM	none	na
14	ANDROGRAPHOLIDE	none	na
15	APRAMYCIN SULFATE	none	na
16	AVANAFIL	none	na
17	BEPHENIUM HYDROXYNAPTHOATE	none	na
18	BETULINIC ACID	none	na
19	BOLDINE	none	na
20	CAPOBENIC ACID	none	na
21	CARYOPHYLLENE [t(-)]	none	na
22	CEFAZOLIN SODIUM	none	na
23	CEFDINIR	none	na
24	CHLORPROTHIXENE HYDROCHLORIDE	none	na
25	CLOXYQUIN	none	na
26	CORTISONE	none	na
27	CRUSTECDYSONE	none	na
28	CYCLOPAMINE	none	na
29	CYCLOTHIAZIDE	none	na
30	CYPERMETHRIN	none	na
31	CYTISINE	none	na
32	DENATONIUM BENZOATE	none	na
33	DERRUSNIN	none	na
34	DIHYDROCELASTROL	none	na
35	DIPLOSALSALATE	none	na
36	DIRITHROMYCIN	none	na
37	DRONEDARONE HYDROCHLORIDE	none	na
38	EBASTINE	none	na
39	EBSELEN	none	na
40	ELLAGIC ACID	none	na
41	EPICATECHIN MONOGALLATE	none	na
42	ERGOTAMINE TARTRATE	none	na
43	ESTRADIOL ACETATE	none	na
44	ESTRADIOL-3-SULFATE, SODIUM SALT	none	na
45	ESTRAMUSTINE	none	na
46	ESTROPIPATE	none	na
47	ETHOXYQUIN	none	na
48	ETHOXZOLAMIDE	none	na
49	FENOLDOPAM MESYLATE	none	na
50	FENSPIRIDE HYDROCHLORIDE	none	na

Node ID	Name of Molecule	Evidence for direct disruption of amyloid fibrils (PMID)	Targeted Amyloid
51	FLAVANONE	none	na
52	FORMONONETIN	none	na
53	GLIQUIDONE	none	na
54	HALAZONE	none	na
55	HIERACIN	none	na
56	HYDROCORTISONE	none	na
57	IODIXANOL	none	na
58	IODOQUINOL	19664688	Abeta42
59	ISOBUTAMBEN	none	na
60	ISOGUVACINE HYDROCHLORIDE	none	na
61	IVERMECTIN	none	na
62	IZALPININ	none	na
63	LANSOPRAZOLE	none	na
64	LOVASTATIN	none	na
65	MEROGEDUNIN	none	na
66	MEROPENEM	none	na
67	METHAZOLAMIDE	none	na
68	METHYLPHENIDATE HYDROCHLORIDE	none	na
69	MONOBENZONE	none	na
70	MOROXYDINE HYDROCHLORIDE	none	na
71	N-METHYLBENZYLAMINE HYDROCHLORIDE	none	na
72	NATAMYCIN	none	na
73	OCTOPAMINE HYDROCHLORIDE	none	na
74	OLSALAZINE SODIUM	none	na
75	ORNIDAZOLE	none	na
76	PALMIDROL [5mM]	none	na
77	PANTOPRAZOLE	none	na
78	PHENYLBUTAZONE	none	na
79	PHENYLETHYL ALCOHOL	none	na
80	PODOFILOX	none	na
81	PREDNISOLONE SODIUM PHOSPHATE	none	na
82	PYRITHYLDIONE	none	na
83	PYROCATECHUIC ACID	none	na
84	QUINOLINIC ACID	none	na
85	SEROTONIN HYDROCHLORIDE	none	na
86	SHIKIMIC ACID	none	na
87	SULFAMETER	25043951	IAPP
88	SULFAMETHAZINE	none	na
89	TANSHINONE IIA SULFONATE SODIUM	none	na
90	THIMEROSAL	none	na
91	THYMOQUINONE	none	na
92	TILMICOSIN	none	na
93	TOLNAFTATE	none	na
94	TRETINOIN	none	na
95	TRICHLOROETHYLENE	none	na
96	TRIMEDLURE	none	na
97	TYROSINE HYDROCHLORIDE	none	na
98	URIDINE	none	na
99	VALSARTAN	none	na
100	VANITIOLIDE	none	na

Supplemental Figure 7

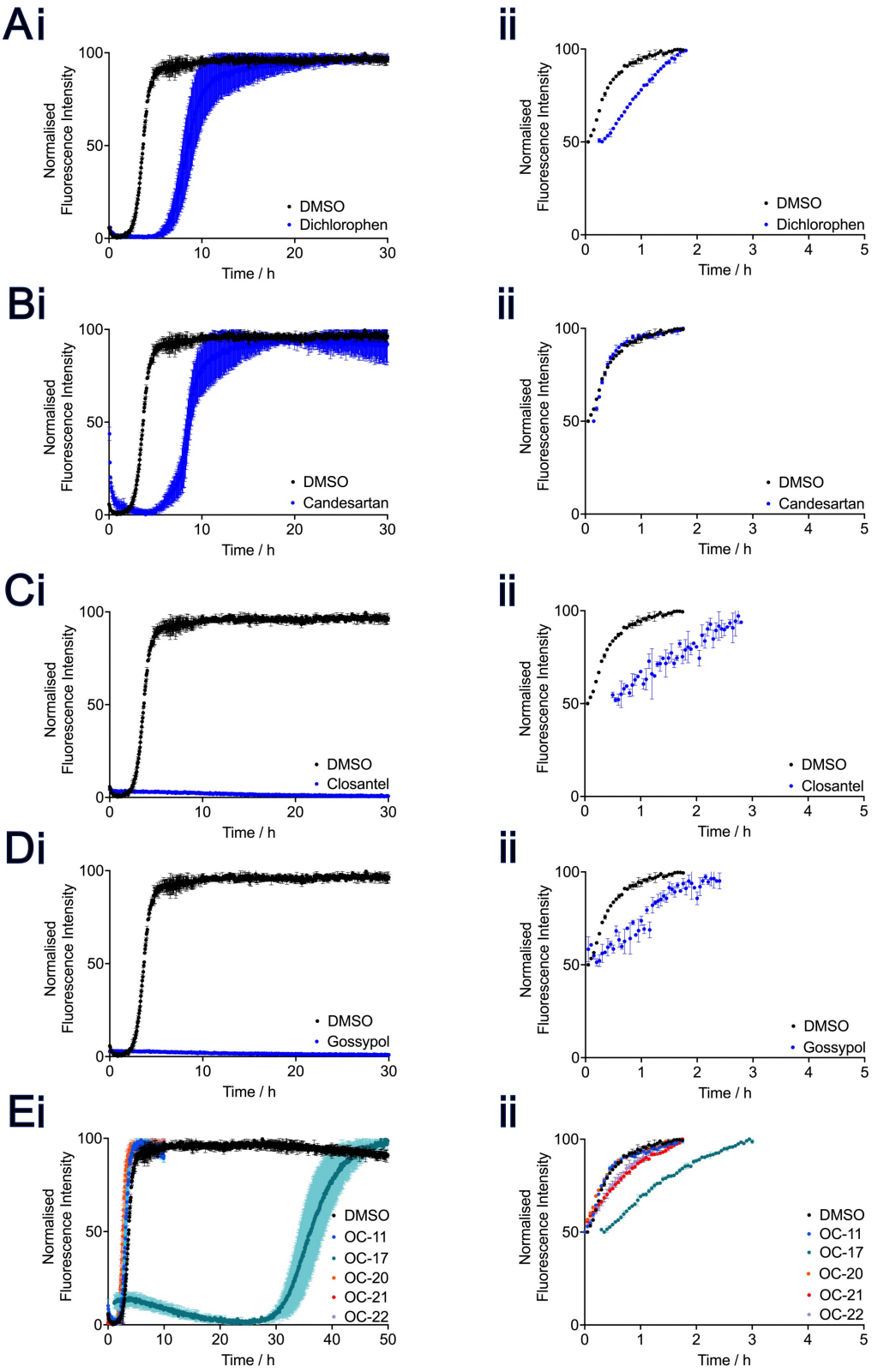

63 **Supplementary Data File 1**

64 **Tab 1 (the screen of RLL1200 for crystalizing small molecules)** contains the information
65 on the RLL1200 library for which we screened for new crystalizing molecules. Red cells
66 on the table indicate that the culture is dead (fewer than 12 animals remaining); orange
67 and yellow indicate that the culture is sick (between 12 and 50 animals), and green
68 indicate that the culture is growing well. OG, over-grown; L, larvae; A, adults. The 16 hits
69 are in the top 16 rows.

70

71 **Tab 2 (16 new crystallizers)** contains the screening and follow-up data for the 16
72 molecules identified as crystallizers along with the associated counts (see Methods and
73 main text for details). Red cells in the table indicate that the culture is dead (fewer than
74 12 animals remaining); orange and yellow indicate that the culture is sick (between 12
75 and 50 animals), and green indicate that the culture is growing well. OG, over-grown; L,
76 larvae; A, adults.

77

78 **Tab 3 (Spectrum Screen for Crystallizers)** contains the information of the Spectrum
79 library for which we screened for new crystalizing small molecules. Only two candidate
80 crystallizers resulted from the screen with dehydrovariabilin being the only reproducible
81 hit.

82

83 **Tab 4 (Spectrum Screen for Suppressors of wact-190 Crystals)**. The hits are shown in
84 the first 85 rows of data. Purple cells on the table indicate that the culture is dead

85 (fewer than 12 animals remaining); gray indicate that the culture is sick (between 12 and
86 50 animals), and green indicate that the culture is growing well. OG, over-grown; L,
87 larvae; A, adults.
88
89 **Tabs 5 and 6-10 (Supplemental Tables 1, and 3-7, respectively)**. We include copies of
90 these tables here to allow for ease of copying the SMILES and other information.
91
92 **Tab 11 (The display item of Supplemental Figure 6b)** is included here to allow for ease
93 of copying any pertinent information.
94
95 **Tab 12 (The physicochemical properties of the wactive library).** The first 48 rows of
96 data show the true positives (crystallizers) from the wactive library.
97
98 **Tab 13 (Student's T-Test comparing the physicochemical properties of the wactive**
99 **library and RLL1200 crystallizers).**